Alma Mater Studiorum – Università di Bologna

School of Science

Department of Industrial Chemistry "Toso Montanari"

Corso di Laurea Magistrale / Master

Advanced Spectroscopy in Chemistry

Classe LM-71 - Scienze e Tecnologia della Chimica Industriale

Molecular organization of n-cyanobiphenyl liquid crystals on a molybdenite surface

Experimental Master Thesis

CANDIDATE

Alexandre Samuel Dumon

TUTOR

Prof. Claudio Zannoni

CO-TUTOR

Dr. Otello Maria Roscioni

First Session

Academic Year 2012-2013

Declaration of Authorship

I, Alexandre Samuel Dumon, declare that this thesis titled "Molecular Organization of n-cyanobiphenyl Liquid Crystals on a molybdenite surface" and the work presented in it are my own. I confirm that:

- This work was done wholly or mainly while in candidature for a research degree at this University.
- Where I have consulted the published work of others, this is always clearly attributed.
- Where I have quoted from the work of others, the source is always given. With the exception of such quotations, this thesis is entirely my own work.
- I have acknowledged all main sources of help.
- Where the thesis is based on work done by myself jointly with others, I have made clear exactly what was done by others and what I have contributed myself.

Signed:_____

Date:_____

Contents

List of Figures

List of Tables

Abstract

The alignement and anchoring of liquid crystals on solid surfaces is a key problem for modern device technology that until now has been treated empirically, but that can now be tackled by atomistic computer simulations. Molecular dynamics (MD) simulations were used in this thesis work to study two films of 7 and 8 n-alkyl-4'cyanobiphenyl (7CB and 8CB) liquid crystals , with a thickness of 15 nm, confined between two (001) surfaces of MoS_2 (*molybdenite*). The isotropic and nematic phases of both liquid crystals were simulated, and the resulting structures characterized structurally.

A new force field was designed to model the interactions between the liquid crystal (LC) molecules and the surface of molybdenite, while an accurate force field developed previously was used to model the 7CB and 8CB molecules.

The results show that the (001) molybdenite surface induces a planar orientation in both the liquid crystals. For the nematic phase of 8CB, one of the two solid/LC interfaces is composed of a first layer of molecules aligned parallel to the surface, followed by a second layer of molecules aligned perpendicular to the surface (also called, homeotropic). The effect of the surface appears to be local in nature as it is confined to the first 15 Å of the LC film. Conversely, for the nematic phase of 7CB, a planar ordering is established into the LC film.

The LC molecules at the interface with the molybdenite appear to align preferentially their alkyl chains toward the solid substrate. The resulting tilt angle of molecules was found to be in good agreement with experimental measurements available in literature.

Despite the fact that the MD simulations spanned a time range of more than 100 ns, the nematic phases of both 7CB and 8CB were found not to be completely formed. In order to confirm the findings presented in this thesis, we propose to extend the current study.

Chapter 1

Introduction

1.1 Aims of the Thesis

The widespread use of liquid crystals (LC) in technology has fuelled a large amount of research in the field, ranging from fundamental experimental investigations to the development of theoretical models able to capture the behaviour of such compounds. Examples of use in technology range from displays to organic fields effect transistors and organic solar cells [49]. LC belong to the self-assembly class of materials, meaning that they are able to self-assemble into ordered phases, which are classified according to their degree of ordering. A nematic phase is characteristic of rod-shaped molecules all aligned along a preferential direction. In the nematic phase the molecules maintain the ability to move as in an isotropic liquid with the additional constraint of keeping the molecular director aligned. In the case of a smectic phase, the molecules are arranged into lamellar structures, with a precise interlayer distance, and display some positional correlation in addition to the orientational ordering.
The majority of the current LC-devices rely on an interface between LC and a solid substrate. Therefore, establishing the molecular basis of the properties of LC at the interface is highly desirable. The change in the properties of a LC due to the interaction with a solid substrate is referred to as *anchoring*. The most important factors influencing the anchoring of LC are:

- Dependence of the LC easy axes (favourite anchoring angle on the surface) on external fields.
- Morphology of the surface [49].
- Chemical interaction between the LC and the surface.
- Wetting of the surface.

It is also well understood that the anchoring phenomena depends on the competition between intermolecular interactions and the interaction between the molecules and the substrate, but also on the morphology of the surface (e.g. roughness).
However, if experimental methods such as Scanning Electron Microscopy (SEM) or X-Ray small angle Diffraction (XRD) prove to be effective to measure the structural properties of LC, they are not suitable to explain the way LC anchor on a given substrate. A substantial help comes from the theoretical modelling.
Molecular Dynamic (MD) and computational simulations are now routinely used to investigate large samples, for example MD simulations were used to predict the phase behaviour of

mesogens composed of spherical nano particles coated with an organic layer [35]. The constant improvement of codes and methods over the past two decades, and the rapid increase of computational raw power have made possible to extensively study systems of increasing size, such as proteins or macroscopic systems [44, 40, 41].
In this thesis, we aim to study the interaction of a well-known class of LCs (7 and 8 cyanobiphenyls) with a solid substrate that is molybdenite (MoS_2). For instance, molybdenite has been widely used as a lubricant, but also been recently shown to be a semi-conducting material, with an electron mobility close to theses of silicon or graphene nano-ribbons [46]. Moreover molybdenite is a common catalyst, used for example for the electrochemical production of hydrogen in water [32].
Recent experimental observations by E.Lacaze et al. have shown that the anchoring of the nCB liquid crystal family on a molybdenite (001) surface is actually a bistable anchoring (two axis of anchoring exist). The analysis of theses easy axis proves that the bistability is actually related to the microscopical structure of the surface. The same surface also prove to induce a weak chirality to a 8CB solution [27, 26, 25].

1.2 Liquid Crystals

Liquid crystals are a state of the matter in between the fully organized crystalline state and the isotropic liquid state. We usually describe this state as a mesophase, or mesomorph state (intermediate shape in greek). The nature of LC phases depends on numerous parameters such as the nature of the mesogene (gene means creator in greek, so here refers to the molecule creating the mesophase), its concentration, the temperature and the pressure.

1.2.1 Historical Background

The discovery of LC dates back to 1888, when Professor Friedrich Reinitzer, an Austrian chemist and botanist, who was then working at the University of Prague, observed a spooky new phenomenon: he was trying to determine the melting point of cholesteryl benzoate when he found that this compound seemed to have two melting points. The crystal melted first into a cloudy liquid at 145 $°C$, and when heating up to 178.5 $°C$, the cloudiness disappeared and he observed a translucent liquid. Thinking this observation was due to impurities, Reinitzer asked another colleague to check his results, but the results were the same.
He contacted then Otto Lehmann, a German physicist expert in the field of crystal optics, who proposed that this cloudy state was a new state in between liquid and crystal, presenting properties of both states. For example, he observed that the properties of the cloudy state are anisotropic, in contrast to those of usual liquids. He found that molecules align to each other when submitted to a weak field, and thus their properties depend strongly on the probed direction.
In 1889 he published the paper *Überfliessende Krystalle* (On flowing crystals) [28], later called 'liquid crystals', but the scientific community was sceptic about the proposed new state, claiming it was just a mixture of liquid and solid states.
We have to wait until the 1960s to observe important studies and applications for LC.
The huge theoretical leap in soft matter physics brought by French scientist Pierre-Gilles de Gennes, who later was awarded a Nobel Prize in physics, in 1991, "for discovering that methods developed for studying order phenomena in simple systems can be generalized to more complex forms of matter, in particular to liquid crystals and polymers" drawn more

attention and provided more tools for the study of LC.
The first liquid crystal display was presented by George Heilmeier in 1968 and was based on the dynamic scattering mode (DSM). The application of a voltage to a DSM display switches the initially clear transparent liquid crystal into a milky turbid state. However, this device required a considerable operating current flow and generated a huge amount of heat. In the same year, the first operating room-temperature nematic phase was observed in the MBBA compound, synthesized by Hans Kelker, but this substance did not qualify for any technological application, because of its small nematic range and the presence of impurities. Today, LC are used in many ways, with application ranging from optics to organic electronic, and even biosensors, made possible thanks to the synthesis of LC with better properties [49]. Among theses new compounds, the class of cyanobiphenyl LC, first synthesized by George W.Gray in 1973, presents remarkable chemical stability, a room-temperature nematic phase, and a large temperature window for the nematic phase. Furthermore their large positive dielectric anisotropy and their strong birefringence make them ideal materials for the manufacture of for twisted nematic cell device.
In figures 1.1 and 1.2 we display the chemical structure of the 7CB molecule, and that of the MBBA molecule.

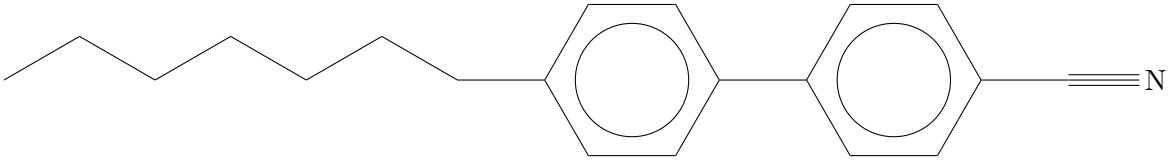

Figure 1.1: 7-cyanobiphenyl molecule

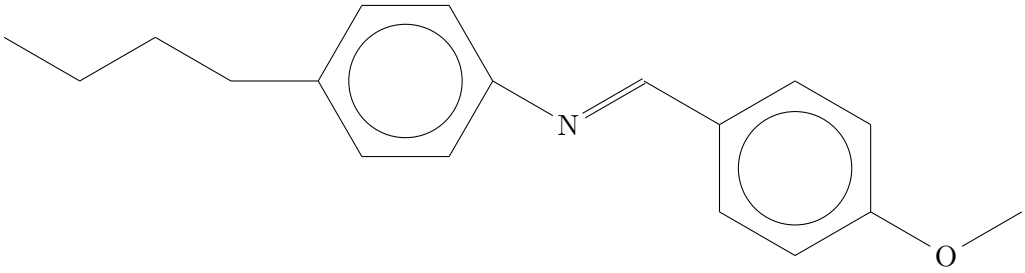

Figure 1.2: MBBA: methoxybenzylidene

1.2.2 Properties of Liquid Crystals

The notion *liquid crystal*, that was first proposed by Lehnann, indicates an intermediate state of matter [4], in between the liquid and crystal states, therefore possessing properties of a liquid (fluidity, coalescence of droplets) but also some crystalline properties (like electrical, magnetic and optical anisotropy, periodic arrangement of molecules in one spatial direction)[4].
Theses properties can be summarized as follow:

- The LC molecule must present an anisotropic shape (e.g. rod-like). The presence of a flat region (benzene rings) in the molecule make it most likely to present LC properties.
- Presence of strong dipoles and easily polarizable groups [4]

Liquid crystals indeed have a very curious morphology: they possess a rigid heart, which must be flat and is usually constituted with one or several aromatic rings and one or more flexible tails, usually aliphatic or perfluorated alkyl chains[4].
Since any torsion within the molecule would cancel this effect, LC must present a rigid core, preventing the molecules to bend too much [4].
Lyotropic crystals are characterized by the presence of an ion, which replaces the rigid aromatic core and on which aliphatic chains are coordinated [4].
If a molecule is amphilic (can make both in Greek), i.e. presents a chemical anisotropy created by a polar and an apolar part, it is likely to posses a LC phase. Aromatic rings are known to stabilize the mesophases by introducing VdW forces [4]. In solution, the polar and apolar part of the molecules tend to align to each other along the other corresponding parts of other molecules, orientating the host molecule, and giving rise to pattern. This is called self-assembly process.
LC can be divided in two families [4]: the thermotropics, whose properties depend on the temperature, and the lyotropics, whose properties depend on their concentration in solution. We will mainly focus on the thermotropics, since the n-CB molecules belong to that class.
LC can present different configurations, as shown in Figure 1.3:

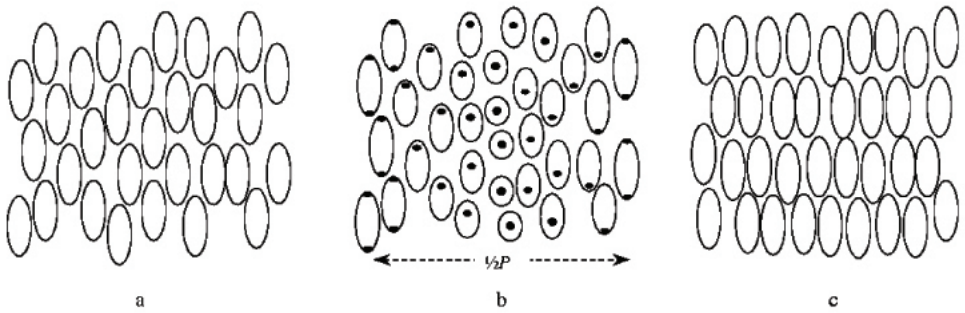

Figure 1.3: Liquid crystals organization: (a) nematic phase, the molecules have the same alignment but their positions are not correlated, (b) cholesteric phase: the molecules have the same alignment which varies regularly through the medium, with a periodic distance of $p/2$, while their positions are not correlated, (c) smectic A phase: the molecules lie in planes and are orthogonal to the planes. Pictures adapted from reference [4]

The nematic arrangement

Among the thermotropic classes of LCs, the nematic ones are the most used industrially (in LCD displays for example). The nematic phase is characterized by a long range organization: the long axis of LC molecules tends to arrange along a particular direction [4]. In absence of external orienting factors, like electric field or interfaces, the medium can present variation of this direction, but locally, all the molecules tend to align along this axis. Theses variations are due to the thermal energy causing fluctuation in orientation, that then diffuse within the sample. This direction is defined by a vector $\mathbf{n(r)}$, and provides the local orientation: this vector is also called *director* [4]. The variation of this director modulates the refractive index of the LC at the macroscopic scale, leading to a strong light scattering and creating the turbid appearance.
There is no positional long-range order of centers of mass in nematic LC. However short-range order may exist in nematic phase. A simplified view of an atomic plan is shown in Figure

1.4((a)).
We never truly observe a perfect arrangement at the microscopic level, since the presence of structural defects results in the formation of strings, from which the nematics take their name: the greek word '$\nu\rho\rho\mu\alpha$' (nema) means thread [4].
Some typical nematic textures are displayed in Fig. 1.4. The first picture was taken under a polarization microscope with crossed polarizer and analyzer. From every defect four dark brushes are generated. In theses directions, the director is parallel to the polarizer [4]. The colors are Newton colors of thin films, i.e. they depend on the sample's thickness.
Figure 1.4b shows a thin film on a isotropic surface [4]. Here the periodic striped structure is a magnificent consequence of the confined nature of the film. It is a result of the competition between elastic and surface anchoring forces. The surface anchoring forces tend to align the LC parallel to the surface and perpendicular to the top surface of the film. The elastic forces work against the resulting 'vertical' distortion of the director. When the film is sufficiently thin, the lowest energy state is obtained with an 'horizontal' director deformations in the plane of the film. This picture shows a 1-dimensional periodic pattern [4].

Figure 1.4: (a) Schlieren texture of a nematic film with surface point defects (boojums). (b) Thin nematic film on isotropic surface: 1-dimensional periodicity. (c) Nematic thread-like texture. Pictures adapted from reference [4]

The phase sequence of the nCB familyare reported in Table 1.1.

n	alkyl chain	Cry	SmA	N
4	C_4H_9	321.2	-	289.6[a]
5	C_5H_{11}	297.2	-	308.2
6	C_6H_{13}	287.6	-	302.2
7	C_7H_{15}	303.2	-	316.2
8	C_8H_{17}	294.6	306.6	313.6
9	C_9H_{19}	315.6	321.2	322.6
10	$C_{10}H_{21}$	317.2	323.6	-
11	$C_{11}H_{23}$	326.2	330.6	-
12	$C_{12}H_{25}$	321.2	332.0	-

Table 1.1: Phase sequence (Cry=crystal, SmA=smectic A, N=nematic) and temperatures of transition (K) for nCB (n=4-12) [17, 30]. Literature data taken from different data sets, with a variance of ±0.5 K.

The nCB LCs with a short alkyl chain (from4 to 7 carbons) present only a nematic phase. In contrast, nCB LCs with a long aklyl chain (from 10 to 12) present only a smectic phase.

Only 8CB and 9CB molecules present two distinct mesophases, which include a nematic and a smectic phase.

Other arrangement

The n-CB family displays nematic phases, and for some of its member also a smectic phase (for n greater than 7). However other arrangements are observed experimentally. The *cholesteric phase* behaves like the nematic phase: it posses a short-range orientational order and no long-range positional order. It differs however from the nematic phase by presenting a periodic variation of the director through the medium. It means that the director varies through the medium, layer by layer, but periodically [4].
The structure of cholesteric LCs is characterized by the distance measured along the axis of rotation of the director, called the pitch, and correspond to the distance between two identical orientations. The pitch is actually only half of this distance, since **n** and **-n** are identical [4].
The nematic phase is actually equivalent to a cholesteric phase with an infinite pitch. Therefore, there is no phase transition between nematic and cholesteric phases in a given material. Furthermore, by doping any nematic LC with an enantiomorphic material one would obtain an optically active cholesteric LC with a rather long pitch [4].
Typical cholesteric LC possess a pitch in the order of hundreds of nanometers,comparable to that of visible light wavelength, giving them a characteristic colors, changing with the direction of observation.
The pitch is very sensible to temperature and applied magnetic or electric field.
Figure 1.5 displays typical cholesteric features.

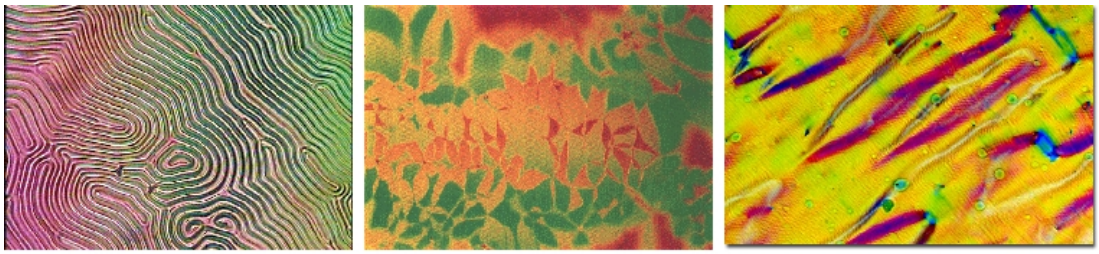

Figure 1.5: (a) Cholesteric fingerprint texture observed under microscope with polarized light. (b) A short-pitch cholesteric liquid crystal between crossed polarizers.. (c) Long-range orientation of cholesteric liquid crystalline DNA mesophases observed under microscope with polarized light. Pictures adapted from reference [4]

The *smectic arrangement* present more degree of order than the nematic one, and can be usually found at lower temperature. Like the nematic phase, smectic take its name from ancient greek $\sigma\mu\eta\gamma\mu\alpha$ (smecta), meaning soap [4]. The smectic phase is indeed observed mainly in soap-like compounds.
Smectic compounds are particular in the sense that they are stratified, i.e. arrange themselves into lamellar structures, with a precise interlayer spacing. In addition to the orientational ordering they also display some positional correlation. Smectic are usually highly viscous fluids, because of the weak interlayer interactions, making possible for the layers to slide on each other [4].
Smectic phases can be split into several groups, depending on the in-plane positional ordering

of the molecules and on the tilt of the long molecular axis with respect to the layer planes. The most common smectic is labelled A. In this arrangement, the long axis of the molecules lye on average orthogonal to the layer plane. Inside the layers, the molecules are ordered randomly. Given the flexibility of the layers, distortions are often displayed by smectic A phases, rising optical patterns known as *focalconic texture* [4]. The phase is uniaxial, since the tilting of the long-molecular axis with respect to the normal is randomly distributed within the bulk. Because of the tilting, a layer can present a thickness lower than the molecules size, but this phenomenon is compensated when considering a bulk sample. Another common smectic phase is labelled smectic C type, and is characterized by a tilt angle different depending on the temperature.
There are other kinds of smectic phases, characterized by tilting angles of the molecular axis. The sequence of phase transitions in a mesogene is summarized in the following list [4]:

- the nematic phase always occurs at at a higher temperature than the smectic phase
- the smectic phases occur in the order $A \rightarrow C \rightarrow B$ as the temperature decreases.
- The kind of smectic depends on the tilt angle of the long-molecular axis to the layer plane

Typical features of smectic LC can be observed in Figure 1.6.

Figure 1.6: (a,b) Focalconic fan texture of a chiral smectic A liquid crystal (c) Focalconic texture of a chiral smectic C liquid crystal. Pictures adapted from reference [4]

When disk-shaped mesogenes orient in a layer-like fashion, the resulting phase is known as a discotic nematic phase. Then, if the disks pack themselves, the phase is called *discotic columnar*. The columns can arrange thyself into hexagonal, rectangular, tetragonal and oblique arrays. Chiral discotic phases can also be observed [4].
Columnar liquid crystals are sorted according to their structural order and column packing. Several features of discotics are displayed in figure 1.8 and 1.9. Typical discotic compounds are shown in Figures 1.7 1.8.

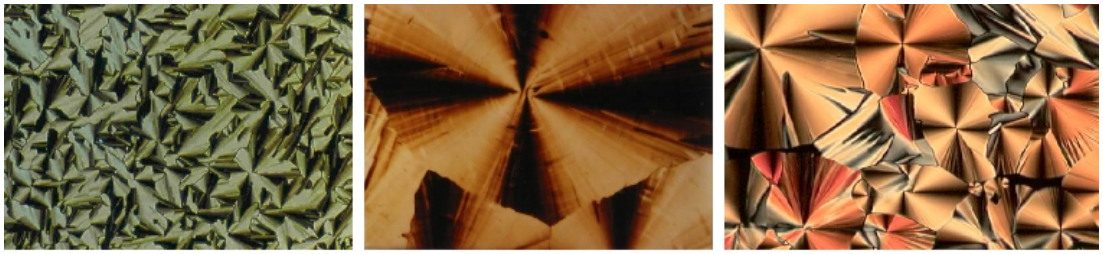

Figure 1.7: (a) hexagonal columnar phase; (b) Rectangular phase of a discotic liquid crystal (c) hexagonal columnar liquid-crystalline phase. Pictures adapted from reference [4]

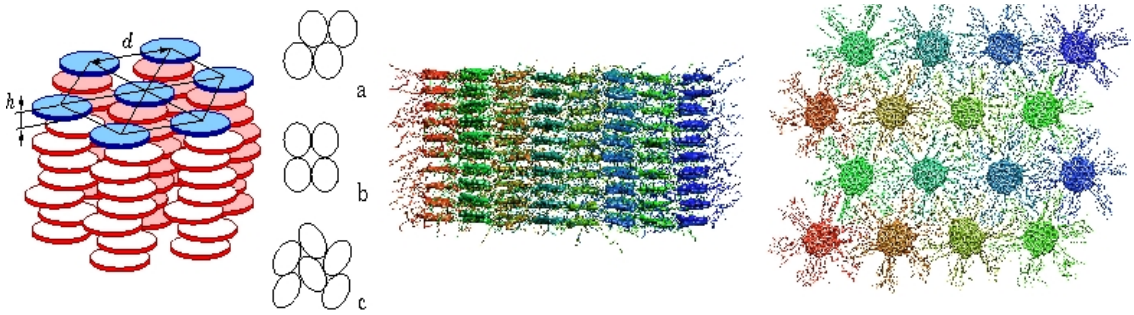

Figure 1.8: Some views of discotics arrangement. Pictures adapted from reference [4]

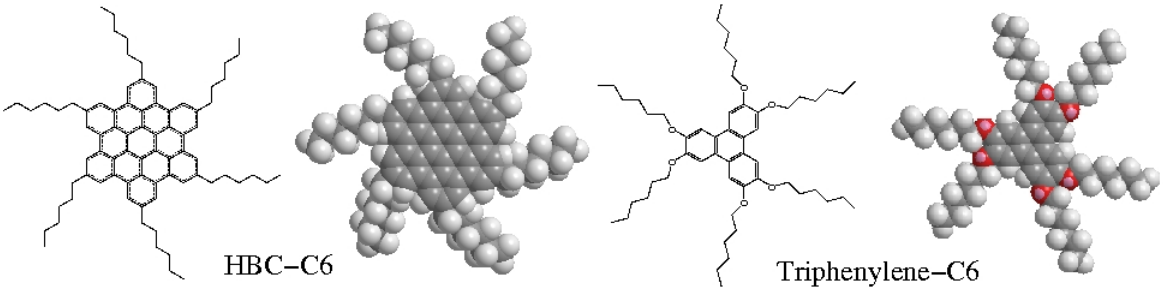

Figure 1.9: Typical discotics: HBC-C6 (left), triphenylene-C6 (right). Pictures adapted from reference [4]

1.3 Anchoring of Liquid Crystals

The molecular organization of LC and other organic functional materials at their interfaces with solid substrate is of high importance for the understanding, the optimization and design of devices such as organic field effect transistors, displays and organic solar cells [49]. On account of this importance, a large amount of empirical data has been collected about the strength of interaction with surfaces (i.e. adhesion), but also on the orientation of LC, this property being referred to as *anchoring*. The orientation of LC molecules at the interface with a solid substrate can be classified into several cases [49]:

- Perpendicular to the surface (also referred to as 'homeotropic').
- Distributed isotropically on the surface (random planar).
- Parallel to the surface with the molecules are aligned along a preferential direction (homogeneous).
- Tilted according to a certain angle (empty cone).
- Tilted from a minimum angle to a maximum angle, occupying all the angles in between (full cone).

However, theoretical methods able to predict the anchoring are lacking. This is a particular problem since the observed empirical data can depend simultaneously on several parameters [49]. E.g. the anchoring direction of a LC on a surface results from the competition between two phenomena: the substrate roughness, whose role was first studied by Berreman [6], and the interactions between the LC and the substrate or between the molecules themselves.
Although, the nCB family is neither chiral or prochiral, surface-induced chiral phases have been reported for nCB on Highly Oriented Pyrolytic Graphite (HOPG) [25] and MoS_2 [25]. In particular, the chiral ordering of 8CB on MoS_2 was found to be confined at the support interface, without propagating toward the sample [25]. The structure is displayed Figure 13. We observe there a head to tail alignment.

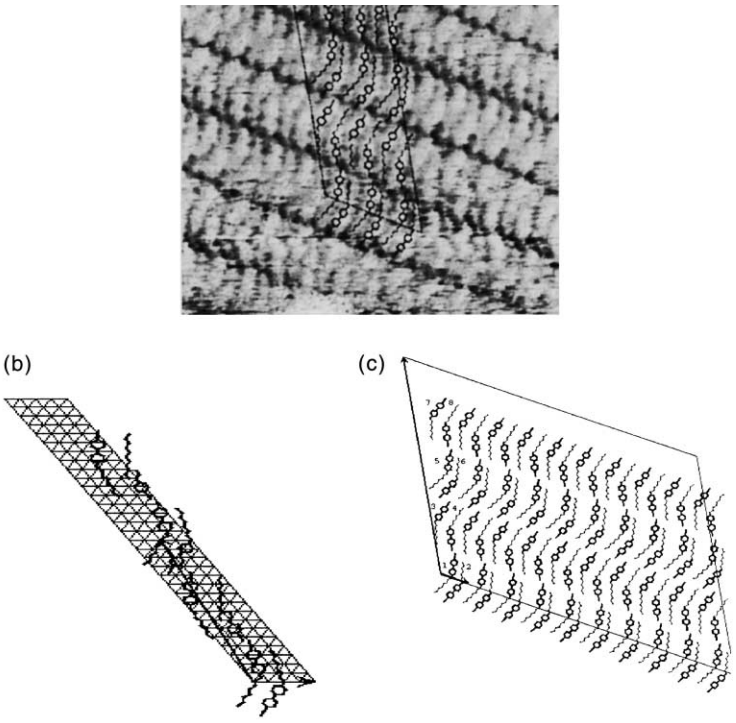

Figure 1.10: 8-CB alignment on a MoS_2 surface. (a) STM image of the 8-CB adsorption. (b) view of the cell. (c) results of the XRD results refinement. Theses pictures have been adapted from reference [24]

This head-to-tail alignment remains stable and was found to occur for 7CB, 9CB and 11 CB, as shown by STM measurements [25]. This experiment shows also that some kinks

appears along the ribbons (cf figure 1.10), resulting from a too large difference between the period of alinement of the substrate and the period of MoS_2 alone [25]. Theses kinks induce chirality into the monolayers, and the rows now present an average angle with respect to the molecules orientation different from 0° or 90°. This phenomenon appears to be governed by the predominance of intramolecular interactions, when the head-to-tail alinement, is governed by strong molecule/substrate interactions.
E.Lacaze et al. reported that the 8CB MoS_2 system possess one easy axe (favored orientations of the LC close to the interface), hence one orientation of adsorbed dipoles or two orientation for adsorbed dipoles and alkyl chains, within the ordered adsorbed surface.
This was observed using XRD, optical microscopy and STM.
The anchoring angle of 8CB on the substrate is of ±17.5° [24].

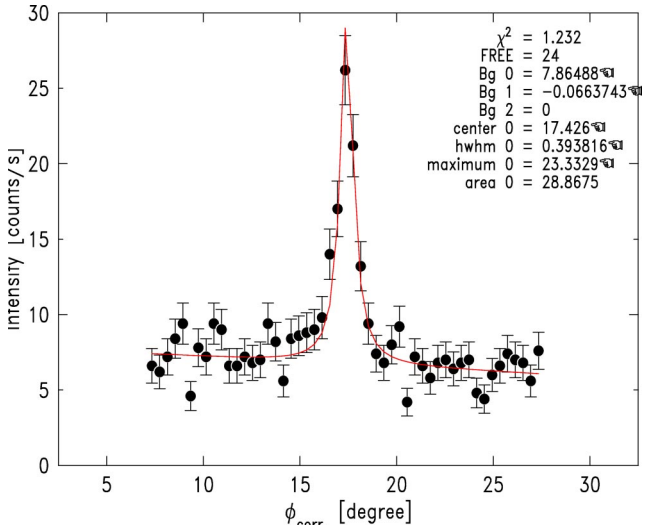

Figure 1.11: 8CB anchoring angle on the MoS_2 surface using XRD [24]

Also, by combining scanning tunneling microscopy (STM) and XRD, Lacaze demonstrated that the 2D single LC were disoriented of 60° with respect to each others, due to the hexagonal symmetry of the substrate. STM shows that the LCs are highly ordered on the surface, with 8CB forming ribbons, as shown in Figure 1.12:

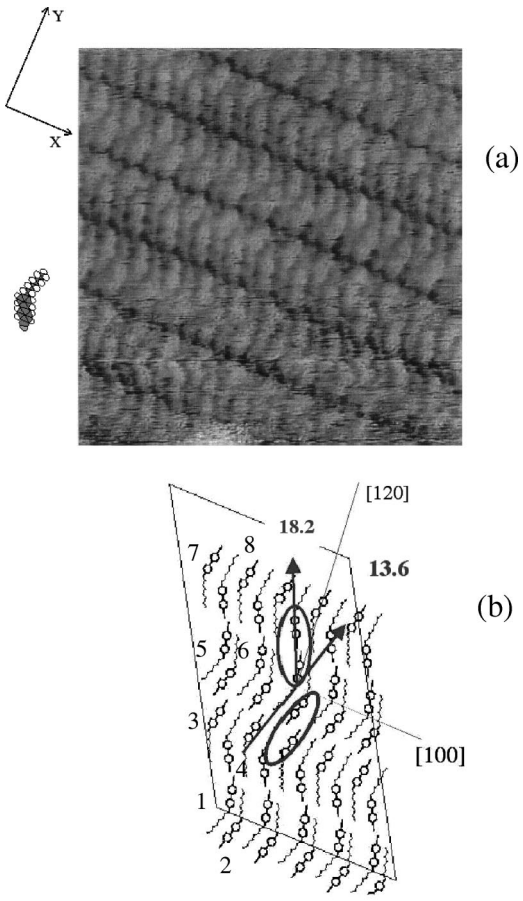

Figure 1.12: 8-CB ribbons on a MoS_2 surface. (a) STM image of the 8-CB adsorption. (b) Microscopical structure refined by XRD

It appears that the dipoles of the adsorbed 8CB molecules arealigned along to two directions: $-13.6°$ and $18.2°$ from the normal to the ribbons.
It is important to notice here that this thesis work slightly larger in scope since we aim to investigate a thin film of LC confined between two (001) MoS_2 surfaces, instead of a mono-layer of LC molecules.

1.4 Physical Properties of Molybdenite

The main physical properties of the MoS_2 are summarized in Table 1.2.

raw formula	MoS_2
molecular mass [5, 60]	$160,09 \pm 0.03$ uma/mol
space group[5, 60]	P_{6_3} /mmc and R-3m
Mohs scale[5, 60]	1- 1.5
density[5, 60]	4.73
melting temperature [59, 46]	1100 °C
conductivity [46]	$2.09 * 10^{-6}$ S/cm
banggap [46]	1.8 eV

Table 1.2: Physical properties of molybdenite

The molybdenite can be found in two forms in nature. One form is rich in iron, is called femolite, and has a raw formula $(Mo, Fe)S_2$[61], the other one is called Rhenium-molybdenite, and has the raw formula $(Mo, Rh)S_2$ [61]. 80% of the molybdenite crystallize in the P_{6_3} /mmc form, and only 20 % will undergo in the form of R-3m [59, 61].
The semi-conductive character of molybdenite is responsible for the metallic gray, aspect of its crystals [59, 61].

Figure 1.13: Mineral of MoS_2

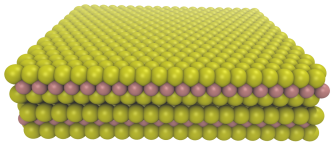

Figure 1.14: Computer model of (001) MoS_2 surface

Molybdenite's genesis is pneumatolytic, i.e. results from the deposition of vapors (pneuma meaning breath in greek) during the final crystallization phase of magma [61]. This generally happens for perigranitic minerals (peri meaning close to in greek). As a consequence it is usually found associated with quartz, iron and nickel sulfurs [61]. It can be also found in some meteorites [59, 5, 61].

Industrial use

Molybdenite crystals are composed of an alternation of Mo and S layers, covalently bound to each others. This structures forms a double sulfur layer engulfing the central Mo layers. Each sheet interacts via Van der Waals dispersion forces, that are weaker than 'covalent' bonds, making easy the sliding of layers [59]. This properties, in addition to the high melting temperature of MoS_2 make the molybdenite a lubricant, used for example in the railroad industry [59, 55].
Molybdenite presents also good properties as a catalyst, for example in reactions on unsaturated sites, like hydrogenation, or cis-trans isomerization [32].
It is also used as an additive during the fabrication of inoxidable steel designed to go in the sea (e.g. super tanker, offshore stations) [59].
Molybdenum is used as a target for the emission of X-rays in XRD devices. Its K_α emission has a wavelength of λ=0,070926 nm.

Figure 1.15 displays a scheme of a transistor based on MoS_2:

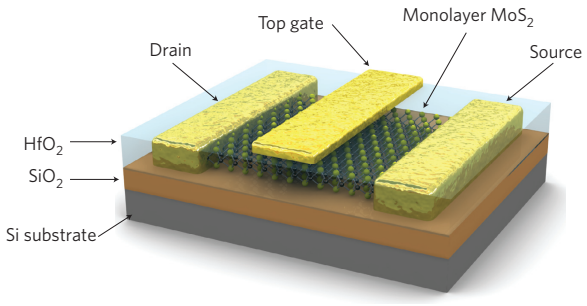

Figure 1.15: Scheme of a transistor based on molybdenite. Figure adapted from [46]

1.5 Aim of the thesis

The aim of this thesis work is to study the molecular organization of two thin films of 7CB and 8CB between two (001) MoS_2 surfaces. Each film is made of 1000 LC molecules, and is approximatively 15 nm thick. Atomistic MD simulations were used to investigate the effect of the surface on the isotropic and nematic phase of the two LCs. The interaction between the LC molecules and the substrate was modelled with a force field tuned to reproduce the absorption energy curve of a 7CB molecule on a (001) MoS_2 surface, computed at a DFT level of theory. The effect of confinement on the structural properties of 7CB and 8CB thin-films is discussed in the central part of the thesis, while general conclusions and suggestions for future work are given in chapter 6.

Chapter 2

Molecular Dynamics Simulations

The molecular dynamics (MD) method was first introduced by Alder and Wainwright in the late 1950's, in order to investigate the phase diagram of a hard sphere system [1]. It was only in 1974 that the first molecular dynamics simulation of a realistic system (water) was performed by Rahman and Stillinger [36, 47].
Even if other theoretical approaches are feasible, MD is still widely used to study molecular systems composed of a large number of atoms, such as liquids, liquid crystals, proteins, membranes, surfaces, and to investigate defects, friction, fractures. MD is also used for drug design and assessment [36]. Figure 2.1 shows two examples of modelisation done using MD. Molecular dynamic is based on the assumption that every atom is represented as a

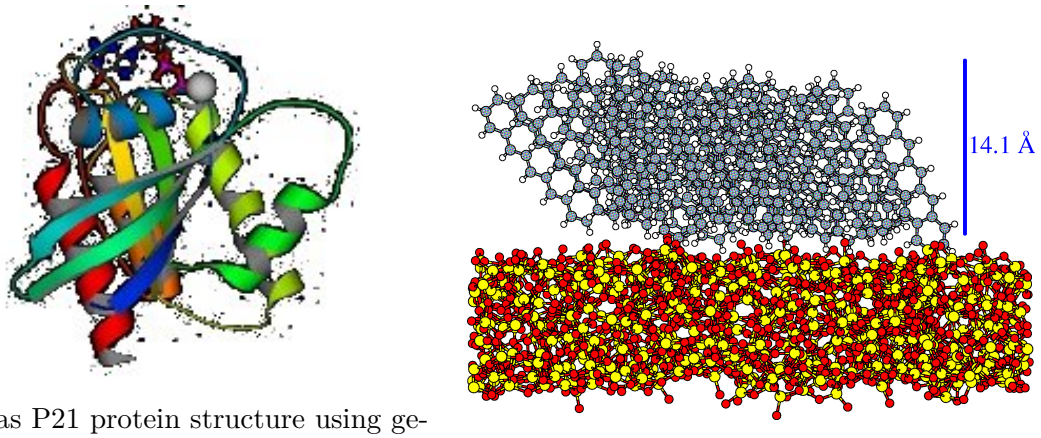

(a) Ras P21 protein structure using geometric optimisation

(b) Pentacene adsorbed on silica glass

Figure 2.1: Example of simulations, taken from [13] and [8]

classical point-like particle. We totally neglect the electronic structure: the contribution of the electrons is not taken into account explicitly during a classical mechanic calculation (MD, Monte Carlo). However, the electronic structure remains important and is used for the determination of the parameters that will be used to model atomic interactions. [36, 42]

2.1 Hamiltonian Dynamics

Hamiltonian dynamics will allow us to follow the trajectories of the particles . This method was first introduced in 1834 as a generalization of Newton's equations for a point particle

subject to a potential function [36, 42].
The Lagrangian of a system is defined as follow:

$$L = T - V \tag{2.1}$$

Where T is the total kinetic energy, and V is the total potential energy. Given a Lagrangian, we can deduce the Hamiltonian of the system using:

$$H(\mathbf{q}, \dot{\mathbf{q}}, t) = \sum_{i=1} n(\dot{\mathbf{q}}_i \mathbf{p_i}) - L(\mathbf{q}, \dot{\mathbf{q}}, t) \tag{2.2}$$

Where $\mathbf{q}$ is a generalized coordinate, $\mathbf{p}$ is the generalized momentum (for most of the studied systems, $\mathbf{q}$=$\mathbf{r}$, $\mathbf{p}$=m$\mathbf{v}$, $\mathbf{v}$ being the velocity of the particle and m its mass). If L is homogeneous, i.e. do not contain the product of different degrees, we have:

$$H = T + V = E \tag{2.3}$$

Where E is the total energy of the system.
In Hamilton's dynamics, the momentum and the position are conjugated variables, meaning the Hamiltonian system possess an even number of dimensions 2N, we need therefore to solve N integrals to specify the trajectory, using Hamilton's equations [36, 42]:

$$\dot{q}_i = \frac{\partial H}{\partial p_i} \tag{2.4}$$

$$\dot{p}_i = -\frac{\partial H}{\partial q_i} \tag{2.5}$$

$$\dot{H} = -\frac{\partial H}{\partial t} \tag{2.6}$$

Theses equations have fixed points when:

$$\dot{q}_i = \frac{\partial H}{\partial p_i} = 0 \tag{2.7}$$

$$\dot{p}_i = -\frac{\partial H}{\partial q_i} = 0 \tag{2.8}$$

i.e. a steady state is reached when $\nabla H = 0$.
An Hamiltonian is *conservative*, which means the energy is invariant with respect to the trajectory the particle follow:

$$\frac{dH}{dt} = \sum_{I=1}^{n} (\frac{\partial H}{\partial q_i}\frac{\partial q_i}{\partial t} + \frac{\partial H}{\partial p_i}\frac{\partial p_i}{\partial t}) = \sum_{I=1}^{n} (\frac{\partial H}{\partial p_i}\frac{\partial H}{\partial q_i} - \frac{\partial H}{\partial p_i}\frac{\partial q_i}{\partial t}) = 0 \tag{2.9}$$

Hamiltonian flows preserve the volume, meaning that the obtained trajectory belong to the micro-canonical NVE ensemble. It means that the number of particles N, the total energy E and the volume V are constant thoughout the trajectory.
In order to integrate the equations of motion, we can use several algorithms. We will present two of them.
The aim of a MD software is to solve numerically the equation of motion at a time t, using the initial velocities and positions $(v(0), r(0))$. However, except for simple cases, the forces F_i are integrated numerically, using a finite time step Δt.

The following algorithm is not accurate but useful to understand the inner working of integration algorithms. We start by defining the derivative of a function:

$$f'(x) = \frac{df}{dx} = \lim_{h \to 0} \frac{f(x+h) - f(x)}{h} \tag{2.10}$$

We can therefore use:

$$f(x+h) \approx f(x) + hf'(x) \tag{2.11}$$

We recall here that the velocity v is the first time derivative of the position and is therefore

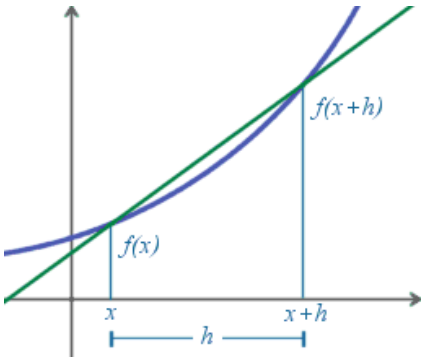

Figure 2.2: Derivative of a function

noted $\dot{r}$, and that the acceleration is the second time derivative of the position, noted $\ddot{r}$, so the first derivative of the velocity. If we set $h = \Delta t$ in (2.11), we obtain:

$$r(t + \Delta t) = r(t) + \Delta t \dot{r}(t) \tag{2.12}$$

$$\dot{r}(t + \Delta t) = \dot{r}(t) + \Delta t \ddot{r}(t) \tag{2.13}$$

As a consequence, by providing the initial velocities and positions, we can compute the initial forces, that are a linear function of r(t). From the force, we find the acceleration, and then we can integrate the first step $0 + \Delta t$. And so on for the following steps.
This algorithm is inaccurate because is a first approximation, and will therefore not lead to correct results.
The method described previously is equivalent to a Taylor expansion truncated at the second term:

$$r(t + \Delta t) = r(t) + \frac{1}{1!}\Delta t \dot{r}(t) + O(\Delta t)^2 \tag{2.14}$$

We could, therefore, expand the series to higher terms as it would increase the accuracy. By expand the series to the fourth term, we obtain:

$$r(t + \Delta t) = r(t) + \frac{1}{1!}\Delta t \dot{r}(t) + \frac{1}{2!}\Delta t^2 \ddot{r}(t) + \frac{1}{3!}\Delta t^3 \dddot{r}(t) + O(\Delta t)^4 \tag{2.15}$$

And

$$r(t - \Delta t) = r(t) - \frac{1}{1!}\Delta t \dot{r}(t) + \frac{1}{2!}\Delta t^2 \ddot{r}(t) - \frac{1}{3!}\Delta t^3 \dddot{r}(t) + O(\Delta t)^4 \tag{2.16}$$

By adding the two equations, we obtain:

$$\dot{r}(t) = \frac{r(t + \Delta t) - r(t - \Delta t)}{2\Delta t} \tag{2.17}$$

We can do the same for the velocity, and obtain the same set of equations, leading to :

$$\ddot{r}(t) = \frac{\ddot{r}(t + \Delta t) - \ddot{r}(t - \Delta t)}{2\Delta t} \tag{2.18}$$

The error is now in the order of $O(\Delta t)^4$. This method is called the Verlet algorithm [56].
The only remaining problem is the first step: since the positions and velocities at time $(t-\Delta t)$ are not known. This can be solved by using the first order approximation for the first step, and then using the Verlet algorithm [56].
The integration step usually varies between 0.1 fs and 20 fs. It has to be small enough to have a good conservation of the energy and big enough for us to follow the dynamical evolution of a system, for a reasonable amount of time, and to maximize the use of hardware resources.

2.2 Statistical Ensembles

An ensemble is a fictive collection of replicas of a macroscopic system. In a statistical mechanical ensemble, each replica is in the same macro-state as the real system, but occupies a different micro-state. [16]
There are several kind of ensembles [16]:

- N V E, called micro-canonical ensemble
- N P T, called isobaric-isothermic ensemble
- N V T, called canonical ensemble

Where N is the number of particles, V the volume, E the total energy, P the pressure, T the temperature. NVE means that the total energy, the volume and the number of particles are constant. And so on for the other spaces [16]. For example, in the NVE ensemble, all the replicas have the same volume, the same energy and number of molecules, but occupy different micro-states that are compatibles with theses constraints.
We then compute the macroscopic properties by summing over all the microscopic states [16].

2.3 Finite size effects

Since the systems studied at the MD level are very small compared to real systems (the factor of comparison being of the order of 10^{17}, if we consider that a mmol sample presents macroscopic properties), we introduce a systematic error from the infinite (bulk) behavior.
To solve this problem periodic boundary conditions (PBC) are introduced as replicas of the simulation box, in every direction, so we actually form an infinite lattice. Figure 2.3 displays such an infinite lattice. [36, 42]
During the simulation, if a molecules moves inside the original box, its periodic images move the same way, so, if one molecules leaves the original box, its image will enter through the opposite face, with the same velocity and orientation. Using this method, the system does not present free surfaces, even if we introduce an additional periodic correlation between the particles. In the case of short range intermolecular potential, this does not represent a problem, since the range of interaction is less than half of the length of the box. We use also the *minimum image convection*: it means that the distance between two particles i and j is defined as the distance between i and the nearest image of j [2]. Thus every

particle i interacts only with the nearest image of another molecule j. In practice, most of the simulations evaluate the potentials using a cut off radius for computational efficiency: each particles does not interact with the nearest image of the N-1 remaining molecules, but with all the molecules within the cut off distance, the interactions with molecules outside this sphere being assumed to be negligible.

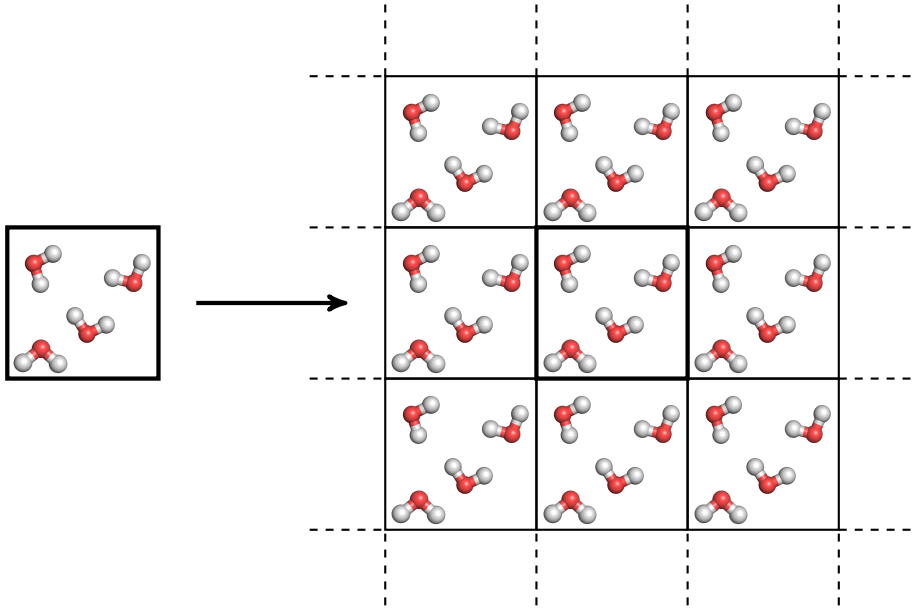

Figure 2.3: Periodic Boundarie Conditions.

2.4 Force Fields

2.4.1 Definition

The energy and forces in a MD simulation are calculated through a given potential energy function, or *force field*, which depends on the relative positions of the atoms and on a set of variables that can be determined either experimentally or using ab-initio calculations [36, 42]. The force field approximation allows us to carry out calculations on much larger samples than with the quantum mechanics calculations, since this approximation is a great simplification over quantum chemistry, which divides the system in terms of electrons, nuclei and wave-functions.
There are different kinds of force fields (FF):

- FF based on harmonic energy functions such as AMBER [23, 58], CHARMM[11] and GROMOS [53], primarily developed to study biological systems [36, 42]
- FF aiming to describe a large amount of compounds: UFF [48], MM3 [3]
- FF created for special purposes such as the modelling of chemical reactions or hydrocarbons modelling [36, 42]: ReaxFF [52], NERD [34], COMPASS [50]

The potential energy functions can be divided into two groups: the bonded and the non-bonded interactions [36, 42]. We will describe theses groups only for the CHARMM/AMBER force fields, which will be used in the simulations presented in this thesis work.

2.4.2 Bonded interactions

3 types of bonded interactions are used in the CHARMM FF [11]: the 1-2 interaction (bond) the 1-3 interaction (angle) and the 1-4 interaction (torsion) [36, 42]. They are displayed in picture 2.4.

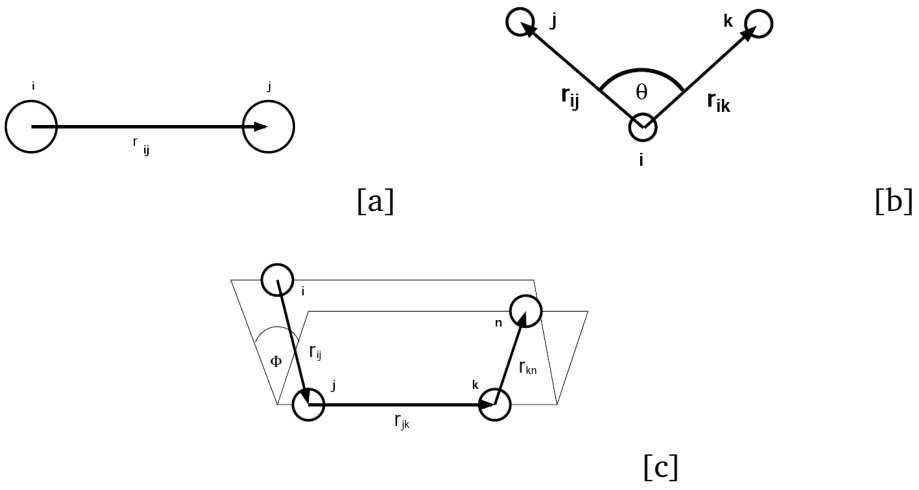

Figure 2.4: Bonded interactions: [a] bond, [b] angle and [c] torsion

The bonded interactions are expressed using the following equations [36, 42, 11]:

- 2-bodies: $\Phi_{bond} = k(r - r_0)^2$. This is the common expression of a spring potential, where k is the spring constant, r the distance between the two atoms, and r_0 the equilibrium distance
- 3-bodies: $\Phi_{three-bodies} = k_\theta(\theta - \theta_0)^2$ where θ_0 and k_θ are the equilibrium angle (resp constant).
- 4-bodies torsion: $\Phi_{torsion} = k(1 + cos(n\Psi + \phi))$ if n > 0 and $k(\Psi - \phi)^2$ if n $= 0$. Ψ is the angle between the plans ijk and jkl (the structure is i-j-k-l), n indicates the periodicity, k is the force constant, and ϕ is the phase shift.

2.4.3 Non-bonded interactions

The non-bonded interactions in AMBER/CHARMM FFs are represented as the sum of a dispersion term and a Coulombic (electrostatic) term. The Coulomb term is given by [11]:

$$\Phi_{elec} = \frac{C q_i q_j}{\epsilon_0 r_{ij}^2} \tag{2.19}$$

Where C is the Coulomb constant, q the charge and r the distance, and ϵ_0 the dielectric permittivity of the vacuum. Bonded atoms do not interact through this term, since their electrostatic interaction has been taken into account in the two-body interaction. A chemical bond is actually a pair of electrons shared between two atoms, which is modelled as a spring in this particular case.

In many ways, electrostatic interactions represent the most challenging problem in computational study since they are by definition long range interactions and difficult to evaluate. Coulomb series is conditionally convergent and need to be evaluated properly to avoid truncation errors.
There are many functions used to compute the Coulombic forces. One is the Particle Mesh Ewald method. This method divides the sample into a grid of points, and calculate the long range interactions using the reciprocal space of this grid, where the long range interactions are fast converging [14]. The short range interactions are computed in the real space, since they converge fast in this space [14]. Therefore, the Coulombic interaction is calculated using equation 2.20 [14]:

$$\Phi_{Coulomb} = \Phi_{short-range} + \Phi_{long-range} \tag{2.20}$$

Another method is the *particle-particle-particle-mesh* (PPPM) method, that maps atom charge to a 3D mesh, and then use Fast Fourier Transform to solve Poisson's equation on the mesh, then interpolates the electric fields on the mesh back to the atoms [18]. It is close to the PME method [12]. The cost of traditional PME scales to $N^{\frac{3}{2}}$, where N is the number of particles, while the PPPM method's cost scales to $N\log(N)$, and is usually faster than the PME method [45].
The equilibrium distance between two proximal atoms results from the balance between an attractive dispersion force and a repulsion force that reflects electrostatic repulsion, as shown in Figure 2.5.

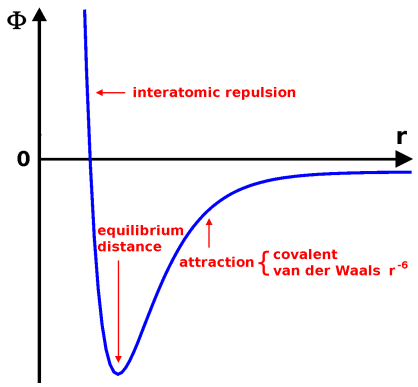

Figure 2.5: Potential of interaction between two atoms

This behavior is described by a dispersion term , which can be modeled via the Buckingham potential or the Lennard-Jones (LJ) potential [11, 29, 9].

$$\Phi_{Buckingham}(r) = Ae^{-Br} - Cr^{-6} \tag{2.21}$$

$$\Phi_{Lennard-Jones}(r) = Ar^{-12} - Cr^{-6} \tag{2.22}$$

Where A, B and C are empirical constants. Usually, the LJ potential is written in the form of [29]:

$$\Phi_{Lennard-Jones}(r) = 4\epsilon[(\frac{\sigma}{r})^{12} - (\frac{\sigma}{r})^{6}] \tag{2.23}$$

This is equivalent to equation (2.22) if $A = 4\epsilon\sigma^{12}$ and $B = 4\epsilon\sigma^{6}$. The two parameters ϵ and σ correspond in fact to physical properties [29]: ϵ has the dimension of energy and is the depth of the potential well, while σ is the distance at which the potential is 0 [29].
We can deduce that the minimum distance, r_{min}, is equal to $r_{min} = 2^{1/6}\sigma \approx 1.12\sigma$, and we

have $\Phi(r_{min}) = -\epsilon$.
The short range 10^{-12} term models the interaction between two atoms brought close together. This part is physically based on the Pauli principle: when the electronic clouds are colliding and overlap, the energy abruptly increases [36, 42, 29]. The 10^{-6} term corresponds to an attractive term acting at long distance. It provides cohesion to the system and originates from Van der Waals dispersion forces rising from dipole-dipole interactions, caused by the fluctuations of electron clouds [36, 42, 29].
The LJ potential is a *two-body* potential, e.g it models the interactions between pairs of atoms. In general we can extend equation (2.21), to include all possible interactions [29]:

$$\Phi = \sum_{i>j} \Phi_{ij}(r_{ij}) \tag{2.24}$$

We use the condition $i > j$ to avoid to consider i-j and j-i as two distinct interactions. As the potential of attraction, decays in $1/r^6$, it can be truncated without affecting the accuracy of the simulation. This distance is called r_{cutoff}.

2.5 Further approximations

In atomistic simulations full-atom (FA) or united-atoms (UA) representations can be chosen to model the molecules[33]. In the latter case, the hydrogens atoms are combined to the heavier atoms they are bonded to (in particular carbon). For example a CH_3 will be a single atom, with a mass of 12+3 =15 amu. In the case of FA representation, all atoms are represented. UA representation allows to decrease the number of interactions that will be computed [33].
It is found that theses united-atoms force fields (UA FF) are as accurate as the full-atom ones (FA FF) when considering phase organizations and static physical properties. UA FF allow to highly decrease the computation time: for example a monomer of $C_{10}H_{14}S$ possess 11 heavy atoms and 14 H, removing them would decrease the computation time by a factor of: $[(11 + 14)/11]^2 \approx 5$ [33], but also they allow to increase the integration step. The typical integration step for FA FF is 1 fs, making the simulation faster, reducing the equilibration time and enhancing the space sampling [33].
We used this approximation for the MD simulations carried out in this thesis work.

2.6 Computation of physical observables

The atomic or molecular positions produced via MD simulations are the starting point for the computation of various physical properties, such as the density and the orientation of the molecules. We use a software developed in Professor Zannoni's group to analyze the MD trajectories and to compute the physical observables.

2.6.1 Orientational order

We define the orientation of the molecule by the angle between its director ($\mathbf{u}$) and the reference axis (here z). This angle is noted β:

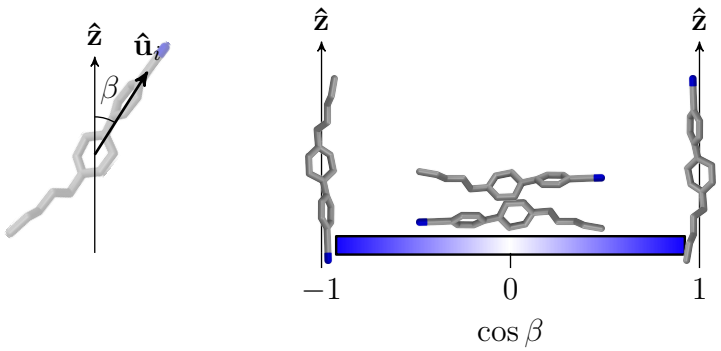

Figure 2.6: Definition of the orientation of a LC. The laboratory axis is z. In color coded pictures, blue is used to represent molecules parallel to z, while the color white is used for molecules perpendicular to the axis z

The position of a molecule can be properly described in terms of three Euler angles (α, β, γ), or only two angles (α, β), called polar angles, as described in Figure 2.7 (provided the molecule displays a cylindrical symmetry) [37]. In the case of the present study, we define the orientation of the whole molecule according to the direction of the C$\equiv$N direction.

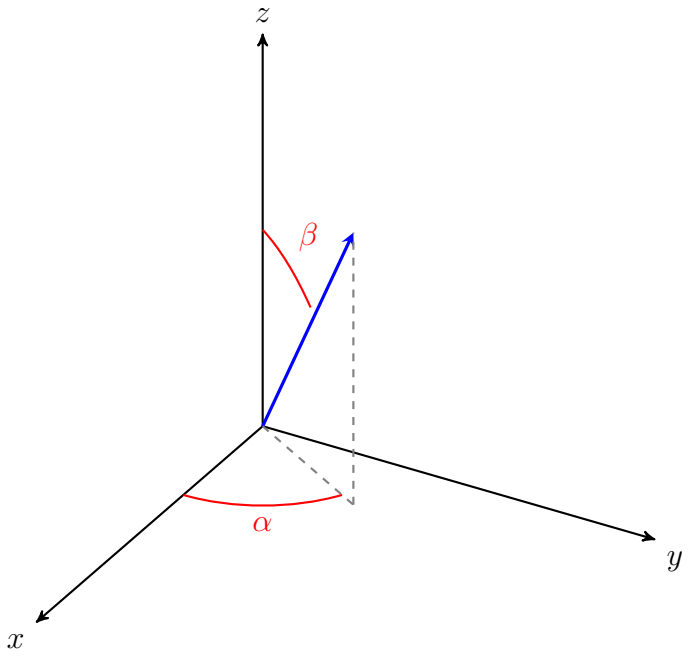

Figure 2.7: Polar angles

In the present case, the probability of an orientation ω, P(ω), is therefore the probability of finding a couple (α,β), so [37]:

$$P(\omega) = P(\alpha, \beta) \tag{2.25}$$

Since we consider here the orientation with respect to the z axis, only the β angle is revelant to describe the orientation, so we have [37]:

$$P(\alpha, \beta) = P(\beta) \tag{2.26}$$

Finally, the distribution of orientation respect the parity constraint, i.e. :

$$P(\beta) = P(\pi - \beta) \tag{2.27}$$

We assume here that $P(cos\beta) = P(\beta)$, and that these functions are normalized.
We can obtain information about the orientation in terms of an adapted system of functions. Such set of functions should represent information that we can obtain from experiment, and has to be orthogonal when integrated over $\mathrm{d}\beta\sin\beta$ (this would mean that one can measure one of this function experimentally without measuring any of the others) [37]. The Legendre polynomials $P_L(\cos\beta)$ are a set of functions filling both conditions [37]:

$$\int_0^\pi P_L(\cos\beta)P_N(cos\beta)d\beta\sin\beta = \frac{2}{2L+1}\delta_{LN} \tag{2.28}$$

This integral is a scalar product of real functions, and it is obvious here that two different Legendre polynomials will have a scalar product equal to 0, meaning they are orthogonal.
Using this set of functions we can expand the distribution of orientation using the following equation:

$$P(\beta) = \sum_{L=0}^{\infty} \frac{2}{2L+1}\langle P_L(\cos\beta)\rangle P_L(\cos\beta) \tag{2.29}$$

Where $\langle P_L(cos\beta)\rangle$ is the average of the polynomial of rank L.
The Legendre polynomials are expressed as follow:

$$P_0(\cos\beta) = 1 \tag{2.30}$$

$$P_1(\cos\beta) = \cos\beta \tag{2.31}$$

$$P_2(\cos\beta) = \frac{3}{2}\cos^2\beta - \frac{1}{2} \tag{2.32}$$

$$P_3(\cos\beta) = \frac{5}{2}\cos^3\beta - \frac{3}{2}\cos\beta \tag{2.33}$$

$$P_4(\cos\beta) = \frac{35}{8}\cos^4\beta - \frac{30}{8}\cos^2\beta + \frac{3}{8} \tag{2.34}$$

$$P_L(\cos\beta) = \frac{1}{2^L}\sum_{k=0}^{E(L/2)} (-1)^k \begin{pmatrix} L \\ k \end{pmatrix} \begin{pmatrix} 2L-2k \\ L \end{pmatrix} (\cos\beta)^{L-2k} \tag{2.35}$$

We notice immediately that the parity of the polynomial of rank L depends on the parity of the integer L, and adding the condition $P(\beta) = P(\pi - \beta)$, the odd terms are discarded, leading to the final expression:

$$P(\beta) = \sum_{L=0}^{\infty} \frac{2}{4L+1}\langle P_{2L}(\cos\beta)\rangle P_{2L}(\cos\beta) \tag{2.36}$$

We can calculate the averages of the polynomials using the equation:

$$\frac{\int_0^\pi P_L(\cos\beta)P(\beta)d\beta\sin\beta}{\int_0^\pi P(\beta)d\beta\sin\beta} \tag{2.37}$$

We only need the first terms to obtain the orientation of the sample relative to one axis:

$$\langle P_2(\cos\beta)\rangle = \frac{3}{2}\langle\cos^2\rangle\beta - \frac{1}{2} \tag{2.38}$$

$\langle P_2\rangle$ provides a quantitative way of assessing the order of the sample [37]. If the sample is composed of totally aligned molecules, $\langle P_2\rangle$ will indeed be equal to 1 ($\cos\beta = 1$), at the opposite, a totally disordered sample, i.e. isotropic, will have $\langle P_2\rangle$ equal to 0 [37]. We have:

$$-\frac{1}{2} \leq \langle P_2\rangle \leq 1 \tag{2.39}$$

$\langle P_2 \rangle = -\frac{1}{2}$ corresponds also to a perfectly aligned sample, but the molecules are aligned in the opposite direction of the reference axis.
It is important to notice here that a $\langle P_2 \rangle$ value can correspond to different orientations, so it is important to use others parameters to provide a complete characterization of an ordered phase. For example, $\langle P_2 \rangle \gg 0$ corresponds either to a conic shape, or to an ellipsoid, using $\langle P_4 \rangle$ will allow us to discriminate both situations: if it is negative, the orientation of the LC will be in a cone shape, otherwise it is an ellipsoid. However we can only measure experimentally $\langle P_2 \rangle$ and $\langle P_4 \rangle$, so we will only simulate and analyze the results of the calculations for theses two parameters [37].

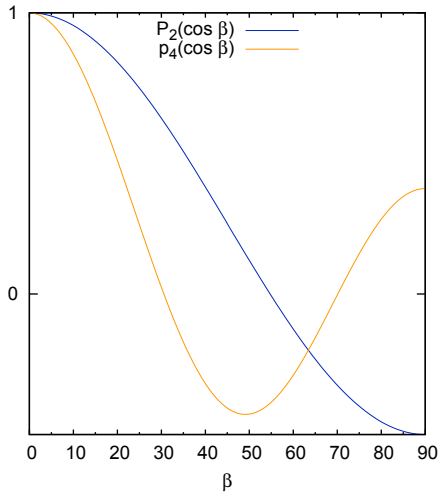

Figure 2.8: Legendre polynomials of order 2 and 4

Experimental determination of $\langle P_2 \rangle$

Experimentally, to determine $\langle P_2 \rangle$, we can compare the probability of absorption through polarized light. This is called the linear dichroism. It relies on the fact that the absorption of the sample will depend on the polarization of the light as well.

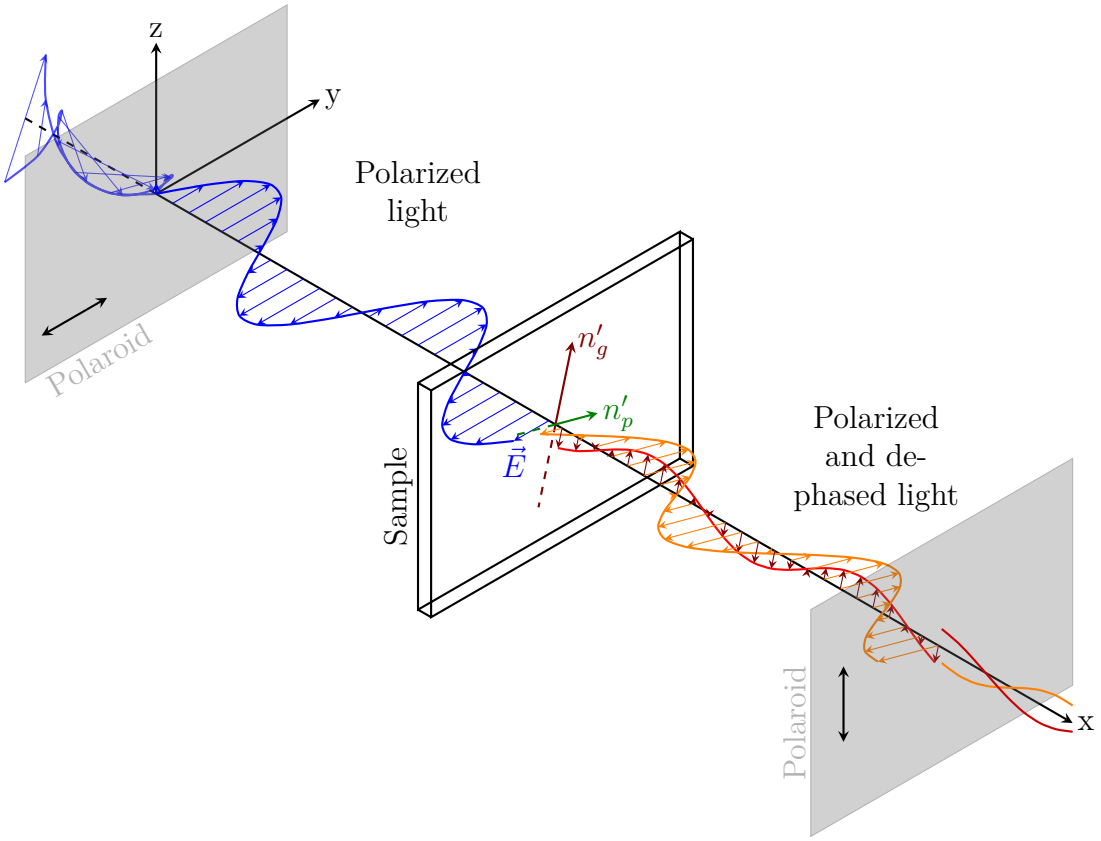

Figure 2.9: Polarization of light. We consider here a monochromatic light, and do not plot the magnetic field, directly orthogonal to the electric field.

This process is governed by the equations [37]:

$$P_i^{abs} \propto \langle [\mu \cdot \mathbf{e_i}]^2 \rangle \tag{2.40}$$

Where P is the probability of absorption for a polarization i, e_i is the polarizer orientation, and μ is the transition moment of the absorption process.

$$P_{\parallel}^{abs} \propto \langle \mu_x^2 + \mu_y^2 \rangle = \frac{1}{3}\mu^2 + \frac{2}{3}\mu^2 \langle P_2 \rangle \tag{2.41}$$

$$P_{\perp}^{abs} \propto \frac{1}{2}\langle [\mu \cdot e_i]^2 \rangle = \frac{1}{3}\mu^2 - \frac{1}{3}\mu^2 \langle P_2 \rangle \tag{2.42}$$

$$\Delta A = P_{\parallel}^{abs} - P_{\perp}^{abs} \propto \mu^2 \langle P_2 \rangle \tag{2.43}$$

The order parameters are computed using a standard procedure for liquid crystals studies: we first build an order matrix $\mathbf{Q}$, summing all over the N molecules of the sample:

$$\mathbf{Q}(t) = \frac{1}{2N} \sum_{I=1}^{N} [3\mathbf{u}_I(t) \otimes \mathbf{u}_I(t) - \mathbf{I}] \tag{2.44}$$

$\mathbf{I}$ being the identity matrix, and $\mathbf{u}_I$ being the reference molecular axis.
The instantaneous value $P_2(t)$, the value of P_2 at a given configuration, is obtained using the eigen values of the $\mathbf{Q}$ matrix [37]:

$$\lambda_- < \lambda_0 < \lambda_+ \tag{2.45}$$

And $P_2(t)$ being equal to the bigger eigenvalue, so to λ_+. If we wait a sufficient long time, the time average $\langle P_2 \rangle$ can be computed using the general expression:

$$\langle A \rangle = \lim_{t_{max} \to \infty} \frac{1}{t_{max}} \int_0^{t_{max}} A(t) dt \tag{2.46}$$

This expression allows us to calculate the time average of a function A. So, replacing A by P_2, we calculate $\langle P_2 \rangle$.
For an isotropic phase we expect a $\langle P_2 \rangle$ value between 0 and 0.2. However, for a smectic or nematic phase, that are arranged phases, we expect $\langle P_2 \rangle$ values higher than 0.6.
$\langle P_4 \rangle$ is computed according to the following equation [37]:

$$\langle P_4 \rangle = \frac{1}{N} \sum_{i=1}^{N} \langle \frac{35}{8} \cos^4 \beta_i - \frac{30}{8} \cos^2 \beta_i + \frac{3}{8} \rangle \tag{2.47}$$

Where β_i is the orientation of the director of molecule i.

2.6.2 Radial distribution function

The radial distribution function (RDF) provides the probability of finding a couple of particles i j at a distance r from each other, relative to the probability expected from a completely random distribution (isotropic), and is defined as follow [33]:

$$g(r) = \frac{V}{4\pi r^2 N} \langle \delta(r - r_{ij}) \rangle_{ij} \tag{2.48}$$

V is the volume, N the number of particles in the system, r_{ij} the distance between particles i and j, and δ the Kronecker delta. In practice, we substitute the δ function by another one equal to one when $r \in [r - \Delta r/2, r + \Delta r/2]$, and zero otherwise. RDF is thus computed as an histogram with a bin width of Δr [33].
RDF is equal to 0 when there are no neighbor particles, and 1 when the correlation is lost (i.e. at long distance). In between, it presents an alternation of peaks corresponding to the coordination shells.
In case of atomistic models theses quantities can be related directly to the structure factors measured using XRD or neutron diffraction [33].
In case of anisotropic systems, it is common to compute the parallel and orthogonal components of the correlation function, to a reference direction z, or to the phase director. The function $\mathbf{g}_{\parallel}(r)$ is useful to identify smectic phases because its layered structure, is revealed by periodic fluctuations, while $\mathbf{g}_{\perp}(r)$ helps do determine in-plane order, for instance in columnar phases.

2.6.3 Positional-orientational order

The computation of the positional-orientational correlation provides quantitative informations about the alignment of molecules within the sample [33]. To compute this quantity we use the following function [33]:

$$\rho(z, \cos(\beta)) = \langle \delta(z - z_i) \delta(\cos \beta - \mathbf{u} \cdot \mathbf{z}) \rangle \tag{2.49}$$

Where β is the angle between the director of the LC and the reference axis (z axis here).
Computing this will provide us a probability of orientation in function of the position in the sample, and will be useful to obtain primary informations about the orientation at the interface or within the sample.

2.6.4 The density

The density of the system is computed by dividing the sample into layers of same thickness, and then compute the density. Since here we are only interested by the density of the LC, we use the following equation:

$$\rho(r) = \frac{m}{V(r)} = \frac{NM}{NaV(r)} \tag{2.50}$$

Where M is the molecular mass of the LC, V the volume of the layer, N the number of LC molecules within the layer, Na Avogadro's number.

2.7 Summary

A flowchart summarizing the work flow of a MD simulation is shown in Figure 2.10.

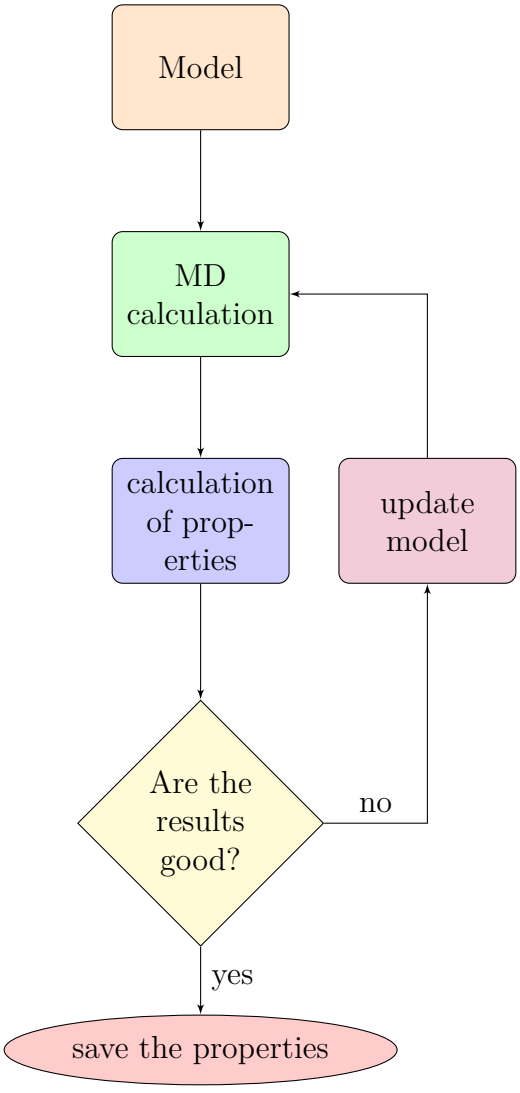

Figure 2.10: Flowchart of a computer simulation

Chapter 3

Computational modeling of MoS_2

In the present chapter we will present the properties of MoS_2, assess the FF used to model the crystal structure and discuss the parametrization of nCB LC on MoS_2 surface.

3.1 Crystal Structure

The bulk structure of MoS_2 was optimized using existing FF which had been already assessed in reference [55]. The parameters of these FF are reported in table 3.1.

Parameters	Becker [55]	Morita [55]	set 8[55]	set 9[55]
Bond coefficients	(D,α,r_0)	(D,α,r_0)	(D,α,r_0)	(K,r_0)
Mo-S	19.94,0.858,2.54	0.398,1.98,2.39	19.945,0.858,2.39	4.3213,2.41
Angle coefficients (K,θ_0)				
Mo-S-M	0.8968,81.67	2.5163,82.00	2.5163,82.00	3.4298,81.67
S-M-S (inter)	0.6356,81.78	2.5163,82	2.5163,82	2.7227,81.78
S-M-S (intra)	0.6356,81.78	2.5163,82	2.5163,82	2.5034,81.78
(ϵ,σ)				
Mo-Mo	1.5549,2.2310	0.8382,2.5510	0.8382,2.5510	0.8382,2.5510
S-S(intra)	0.2981,3.0023	0.0019,3.3695	0.0606,3.3695	0.0606,3.3695
S-S(inter)	0.1656,3.0138	0.0019,3.3695	0.0606, 3.3695	0.0606,3.3695
Mo-S	1.3802,2.9028	0.0399,2.9318	0.0399,2.9318	0.0399,2.9318
partial charge				
Mo	0.734	0.76	0.76	0.76
S	-0.367	-0.38	-0.38	-0.38

Table 3.1: Different set of parameters for MoS_2. Bond coefficient refer to a Morse equation ($\Phi = De((1-exp^{-a(r-r0)})^2-1)$), D(kcal/mol), α (kcal/mol) and r_0 (Å). The potential labelled set9 uses an harmonic bond coefficient: $\Phi = K(r-r_0)^2$ where K is the bond constant, in $kcal.\mathring{A}^{-1}$, and r_0 is the equilibrium distance. The angles are in degree, the distances in $\mathring{A}$, the energies in kcal

Selection of the FF

The bulk structure of MoS_2 was optimized with the program GULP [15], using the FF reported in Table 3.1. The crystal structure of MoS_2 is hexagonal. A comparison between

the experimental crystal structure of MoS_2 and those optimized with different FFs is reported in Table 3.2.

	V ($\AA^3$)	a ($\AA$)	c ($\AA$)
Experimental	106.35	3.1604	12.2950
Becker	119,00	2.9722	15.5548
Morita	88.95	2.9877	11.5060
set8	95.44	3.0104	12.1608
set9	99.05	3.0512	12.2857

Table 3.2: Comparison between the experimental structure of MoS_2 and the structure optimized with the FF reported in table 3.1

The best agreement between the computed values and the experimental structure has been obtained with the FF Becker and the one labelled 'set 9'.
However, since the FF were optimized to reproduce the structural properties of molybdenite, they are not suitable and optimum to compute the interactions between the surface and an organic molecule. We need therefore to derive a new FF to model accurately the LC/MoS_2 interaction.
The (001) MoS_2 surface was created as a 5x6 supercell, starting from the crystal structure optimized with the Becker FF. The structure of (001) molybdenite was optimized with the program GULP [15]. The resulting structure was kept fixed in all subsequent MD simulations. The optimum thickness of the supercell was determined according to the following procedure:

- Preparation of samples of different thickness (from 1 to 10 layers).
- Calculation of the standard deviation σ of the electrostatic potential above every sample. The program GULP was used to compute the electrostatic potential using point charges taken from the Becker FF.
- Plot of σ versus the thickness of the slab.

The thickness at which the standard deviation σ become constant gives the optimum thickness. As shown in figure 3.1, the optimum thickness is reached with 3 atomic planes. However, the variations of the mean value of the electrostatic potential are in the order of 10^{-5} kcal/mol, well below the thermal fluctuations experienced by the system at the temperatures explored in this work. Therefore, a slab composed of two atomic planes was used as it provides accurate electrostatic interactions with the smallest number of atoms.

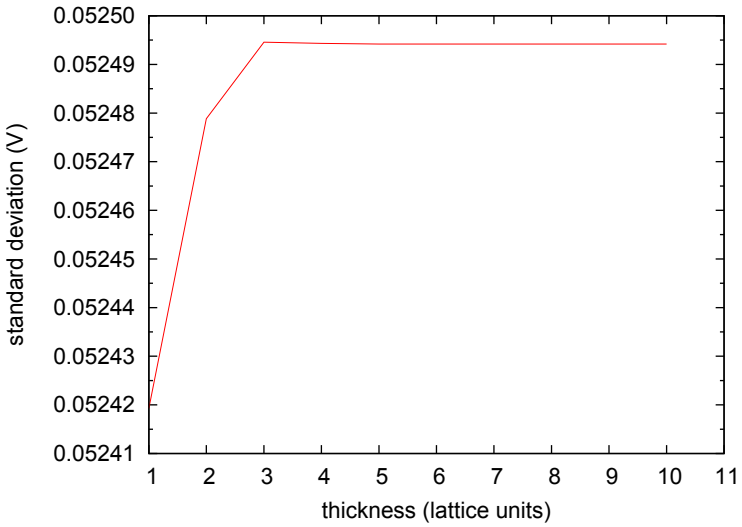

Figure 3.1: standard error of the electric field in function of the thickness of the surface, in atomic plane unit.

3.2 Interaction with organic molecules

The optimization of FF parameters for Mo and S was done by fitting the curve of absorption of a 7CB molecule on MoS_2, obtained using DFT calculations.

3.2.1 Density Functional Theory calculations

The Density Functional Theory approximation (DFT) is a quantum mechanic method used in physic and chemistry to investigate the electronic structure, mainly of the ground state, of many-body systems (atoms, molecules). Its basic is that the energy is a functional of the electron density of the system. A functional is a particular function, that attribute a scalar value to a function. This technique is very popular, because it gives accurate results at a relatively small computational cost. However DFT is not suited to study samples as large as those investigated in this thesis (the DFT simulation of a single 7CB molecule at different distances from the surface took 2 month on a dedicated server, while the MD simulation of 1000 LC molecules on a bigger surface took 11 days on the same machine).
The basic equation of quantum mechanics is the Shrödinger equation:

$$\hat{H}\Psi = [\hat{T} + \hat{V} + \hat{U}]\Psi = E\Psi \tag{3.1}$$

Where $\hat{H}$ is the Hamiltonian operator, $\hat{T}$, $\hat{V}$, $\hat{U}$, are respectively the kinetic energy, potential energy and internal energy operators, and Ψ the wavefunction of the system. Provided that the wavefunction is normalized, the particle density $\vec{n}(r)$ is defined as follow:

$$\vec{n}(r) = N\Psi^*(\vec{r}, \vec{r_2}, \cdots, \vec{r_N})\Psi(\vec{r}, \vec{r_2}, \cdots, \vec{r_N}) \prod_{i=1}^{N} \int d^3 r_i \tag{3.2}$$

Since this operation can be reversed, providing the ground state particle density $\vec{n}_0(r)$, we can obtain the ground state wavefunction Ψ_0. A unique density will provide a unique wavefunction.

Periodic DFT calculations were carried out with the program CASTEP [10]. A 8x8x1 supercell was used to model the (001) MoS_2 surface, coupled with a vacuum thickness of 15 Å used to minimise the interactions between the periodic images of the slab. A cut-off energy of 180 eV was used to construct the plane-wave basis set, with Vanderbilt ultrasoft pseudopotentials [54] and the Perdew-Burke-Ernzerhof (PBE) generalised gradient-corrected functional [38]. Semi-Empirical dispersion-interaction corrections were used to take into account for the Van der Waals interactions between the (001) MoS_2 surface and the 7CB molecule [31]. The value of these parameters ensured fully converged total electronic energies and atomic forces.
We simulated the absorption of the 7-CB on the surface at the DFT level of theory, in two configurations: orthogonal and parallel to the surface. We then fitted the obtained data using a Morse potential function. The fitting parameters can be found in table 3.3:

	parallel configuration	homeotropic configuration
De (eV)	27.1	10
a ($\AA^{-2}$)	0.91	0.27
x_0 ($\AA$)	3.51	3.29

Table 3.3: Morse potential parameters fitted on the DFT absorption energy curves.

We used the fitted Morse curves instead of the DFT absorption curves to identify unequivocally the absorption distance of the 7CB molecule. The DFT calculations are indeed discrete calculations, meaning they only calculate the energy for discrete distances, and are therefore not continue. Moreover, they present also abrupt variation. The fitting allow us to have smoother and continue curves.

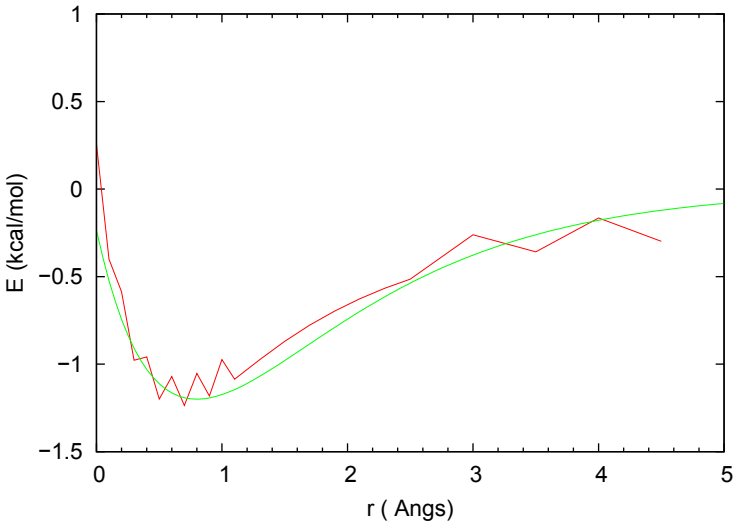

Figure 3.2: Raw plot of the DFT calculations of the absorption of the 7CB in an homeotropic configuration on the molybdenite surface. The points have been joined in order to have a curve easier to understand. The green curve represent the Morse fitting.

3.2.2 Force Field optimization

The interaction between nCB and the surface has been modelled with a LJ potential in the MD simulations. Therefore the LJ parameters for Mo and S were fitted to reproduce the

absorption energy curves of 7CB on MoS_2 computed at the DFT level of theory.
The evaluation of LJ interaction between a molecule and the surface involves a polynomial function with many terms [1], therefore an analytical solution of this problem is out of reach. Instead, we used a trial and error process to optimize LJ parameters, which consists in a systematic variation of each parameters, followed by an evaluation of the corresponding absorption energy curve, carried out with the program NAMD [39].
We found that improving the agreement with the parallel configuration made the agreement with the orthogonal one worse, and vice versa. After a certain number of iterations, we found the best parameters, which are reported in Table 3.4.

	Original Becker	improved parameters
ϵ		
Mo	1.2469	1.4
S	0.4069	0.001
σ		
Mo	1.2521	1.79691
S	1.6914	2.8

Table 3.4: Comparison between the original LJ parameters and the fitted parameters used to represent Mo and S atoms

A graphical comparison between the 7CB/MoS_2 absorption curves obtained from DFT calculations and with a LJ potential function are shown in Figure 3.3

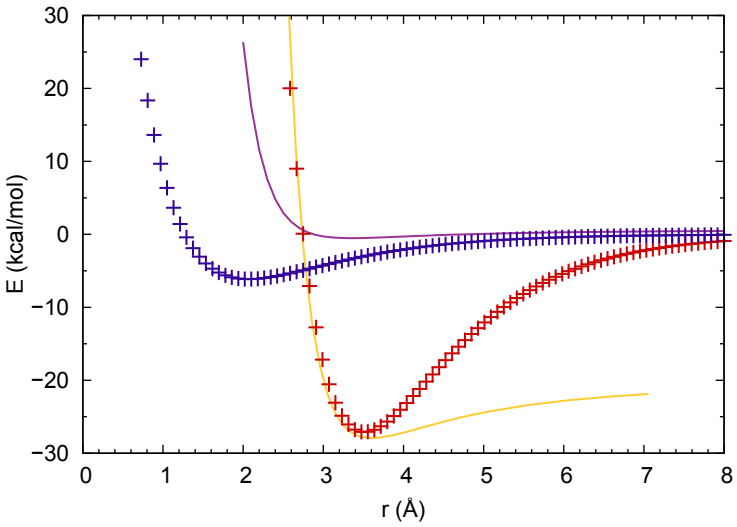

Figure 3.3: Comparison between the absorption of 7CB on MoS_2 in two different configurations: parallel (red cross for the DFT curve and orange line for the LJ curve) and orthogonal (blue cross for the DFT calculations and purple line for the LJ curve).

This is the best set of parameters we could find, and is the one we will use for the simulation, along the set we found using a mathematical fit.

[1] In fact, the terms evaluated correspond to all the pairwise interactions between every atom in the 7CB molecule and all the atoms in the MoS_2 surface within the cut-off distance

Chapter 4

Computer simulations of 8CB on MoS_2

4.1 Introduction

In this chapter we discuss the morphology of a thin film of 8CB confined between two (001) surfaces of MoS_2. The LC phase is described with a force field which has been optimised to reproduce the thermodynamic proprieties of several cyanobifenyl LC [51]. Properties such as phase transition temperatures and density are reproduced accurately. Furthermore, the UA approximation makes the MD simulations computationally less demanding. The study of the molecular organisation of 8CB at the interface with a solid substrate is part of an ingoing study aimed to characterise at a molecular scale the morphology and the orientation of nCB LC on various surfaces, such as amorphous and crystalline silicon dioxide [49] and hydrogen-terminated silicon [43].

4.2 Computational details

MD simulations of the 8CB/MoS_2 system were carried out in the NPT ensemble, using a Langevin barostat to control the pressure and the temperature. The sample studied here is composed of 1000 8CB molecules and a slab of molybdenite represented as a 20x20x2 supercell of the (001) surface. The surface area of the molybdenite is 30.6 nm^2, and the atoms of the molybdenite slab were kept fixed during the MD simulations.

The isotropic phase of 8CB was simulated at 325 K, while the nematic phase was formed by cooling the sample at 310 K. The parameters of the FF used to describe the 8CB (and the 7CB, in the next chapter) are reported in table 4.1.

	m (uma)	ϵ (eV)	σ ($\AA$)
C3	15.024	0.1050	2.050
C2	14.016	0.0705	2.035
Cd	13.008	0.0708	1.950
Ca	12.000	0.0708	1.950
CY	12.000	0.0860	1.908
NY	14.010	0.1700	1.824

Table 4.1: Atomic mass and Lennard-Jones parameters used to describe the inter-atomic interactions of nCB. The atomic charges (not reported here) are specific for every molecular type [51].

An example of the use of the different atom types in this FF are represented in Figure 4.1.

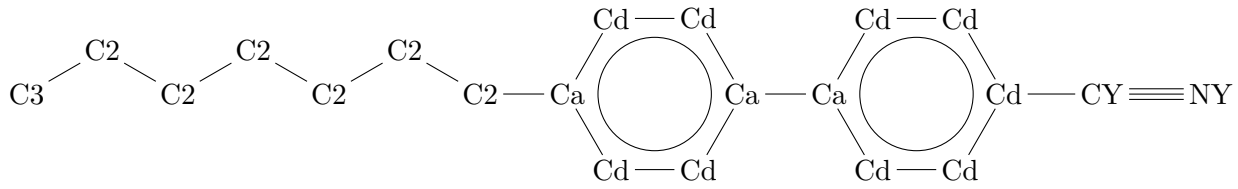

Figure 4.1: Representation of the atom types used by the FF representing the nCB [42].

The interactions between the LC and the molybdenite surface were modelled with a custom FF, whose derivation is discussed in Chapter 3. The atomic charges for sulphur and molybdenum atoms are taken from reference [55].

Two algorithms were used for the temperature control: the Langevin algorithm for the first 130 ns of the simulation, and a velocity rescaling algorithm for the remaining part of the simulation. The velocity rescaling algorithm resulted in faster dynamics and was therefore used to speed-up the production time of the nematic phase of 8CB. A pictorial view of the sample of 8CB/MoS_2 is displayed in figure 4.2.

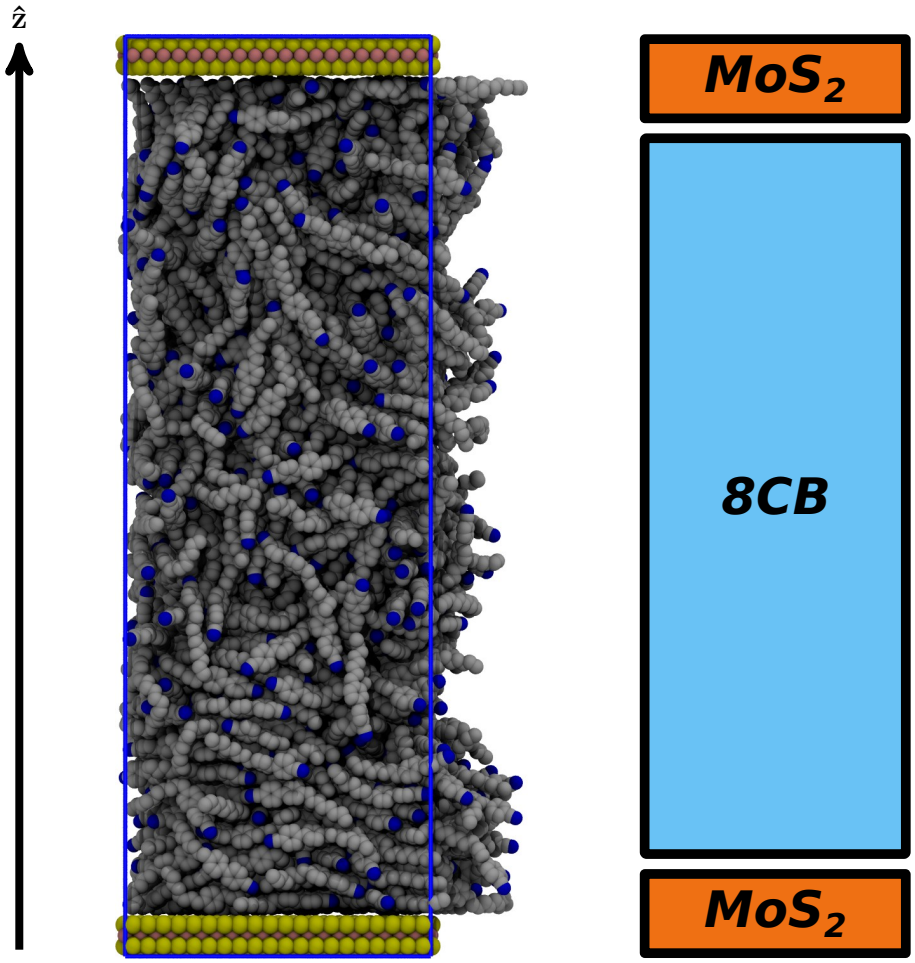

Figure 4.2: Lateral view of a sample of 1000 8CB molecules confined between two (001) MoS_2 surfaces.

4.3 Results and Discussion

4.3.1 Isotropic phase

When performing a MD simulation, one must control the total energy. Once the total energy of the sample is constant for a period of time of the order of the molecular relaxation time, the sample can be considered equilibrated. The isotropic phase of 8CB was simulated for a total time of roughly 50 ns, of which the first 35 ns were used to reach thermal equilibrium and the remaining 35 ns for data production. Figure 4.3 displays the total energy of the 8CB thin film during MD simulations of the isotropic and nematic phases. For the nematic phase, roughly 110 ns were necessary to reach thermal equilibrium. The difference between the equilibration times of the two phases can be ascribed to the fact that for the nematic phase to form, the 8CB molecules need to undergo a coordinated transition in which the molecules align locally their director. The kinetic energy is related directly to the temperature via the equation:

$$\langle K \rangle = \frac{3}{2} k_b T \tag{4.1}$$

where k_b is the Boltzmann constant, T the temperature and $\langle K \rangle$ the average kinetic energy. Therefore, a small temperature implies longer molecular reorientation times.

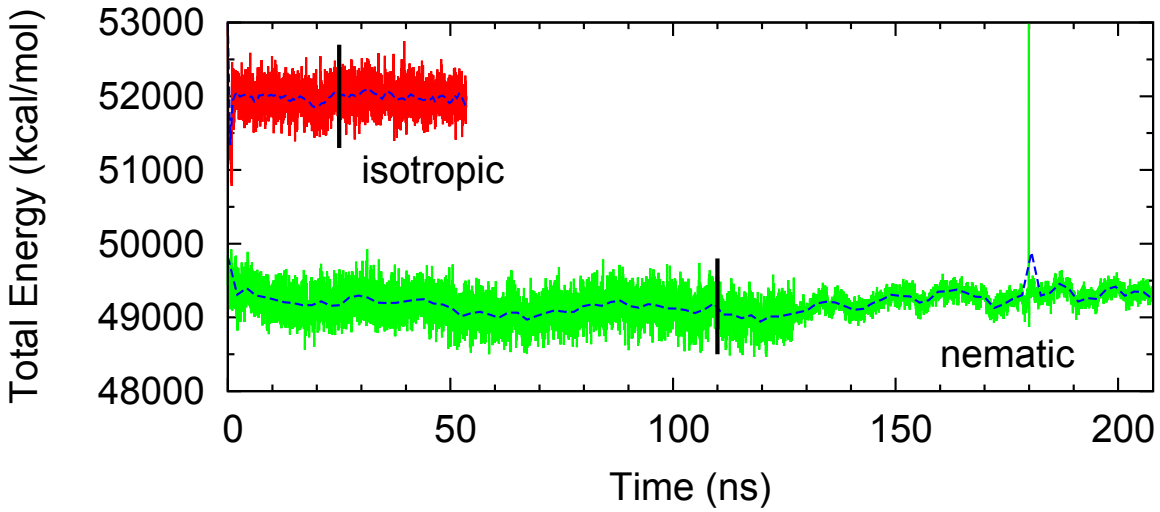

Figure 4.3: Total energy of the 8CB/MoS_2 system at 325 K (red line, isotropic phase of 8CB) and at 310 K (green line, nematic phase). Dashed lines show the mean value of energy, while the vertical black lines mark the beginning of the production phase in each MD trajectory.

The physical observables used to characterize the film of LC have been computed with a program developed in the group of Prof. C. Zannoni, using the MD trajectories referring to the production time.
Since the film of 8CB is confined between two identical surfaces of molybdenite, symmetric features are expected for the two interfaces of the LC.

Density Profile

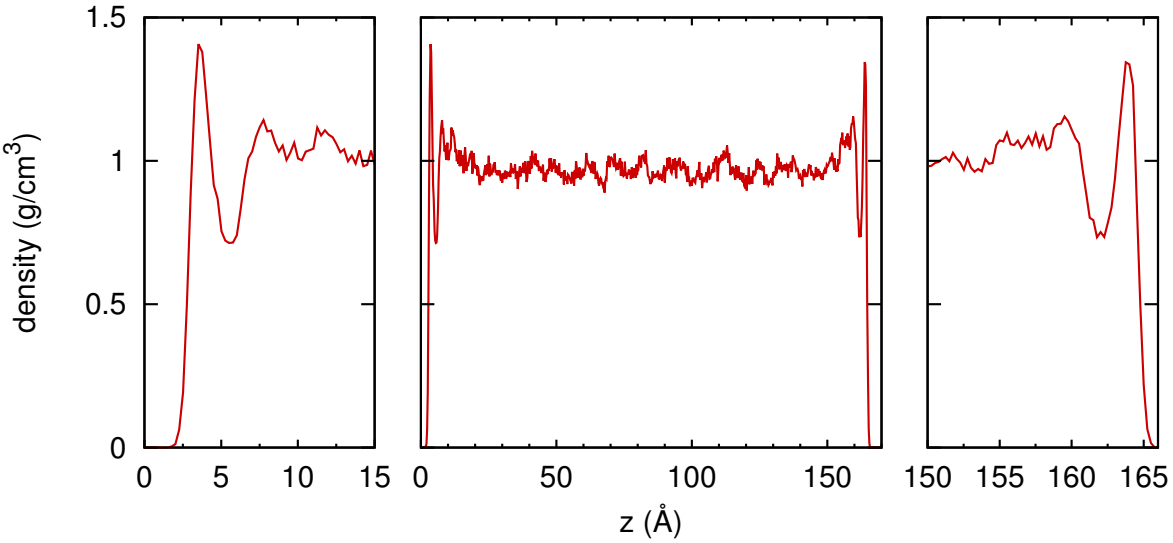

Figure 4.4: Density $\rho(z)$ of 8CB at 325 K across the film (middle panel) and at the interfaces (left and right panels), with respect to the normal at the surface z.

Figure 4.4 shows that the density $\rho(z)$ of 8CB is uniform across the bulk. The interface between 8CB and (001) MoS_2 presents a strong peak, followed by two smaller peaks of decreasing intensity. Theses oscillations corresponds to three successive layers of 8CB molecules coming in close contact with the crystalline surface. From the density profile of the sample we can measure the approximate thickness of the 8CB film, which is 160 Å at 325 K.

Orientation of Molecules

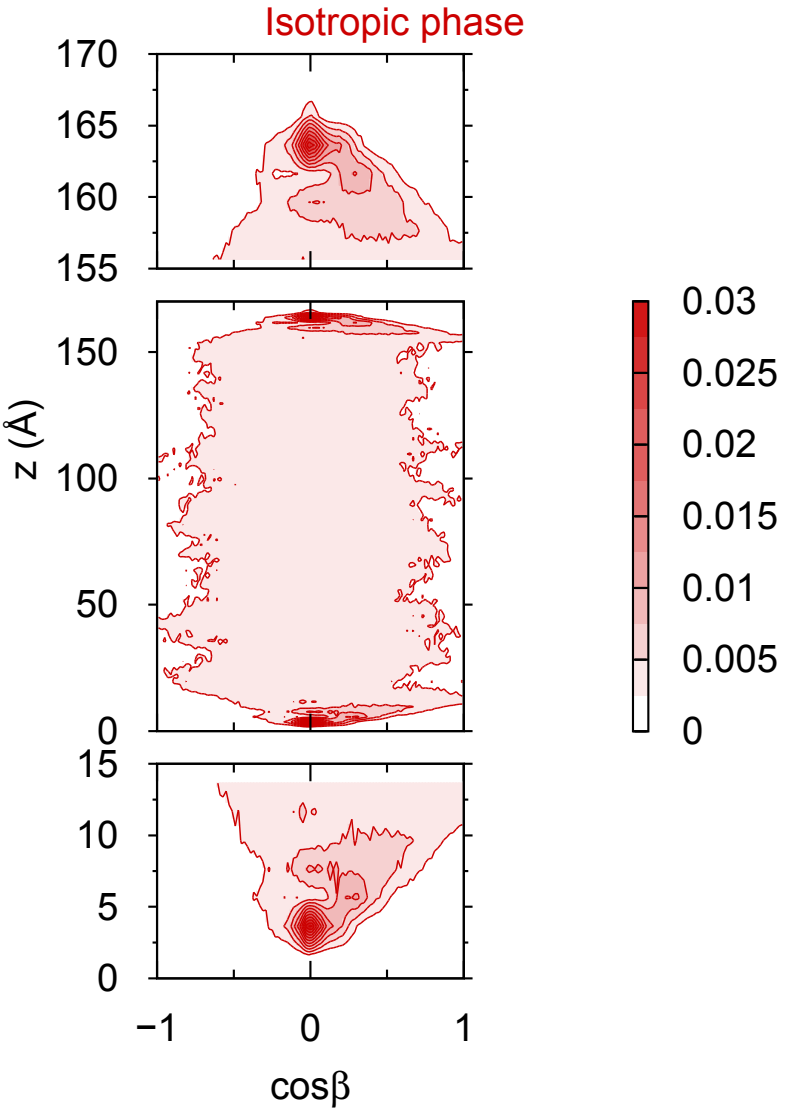

Figure 4.5: Red-shaded contour map of the probability distribution $P(z, \cos\beta)$ of the 8CB film at 325 K. The top and bottom panels show a close-up of the function at the 8CB/MoS_2 interface.

The orientational-positional distribution function $P(z, \cos\beta)$ shows the probability of finding a molecule in a given orientation at a position z. The orientation of each molecule is defined in Figure 2.6 in terms of a vector pointing from the molybdenite surface toward the *centre* of the sample. However, for one of the two surfaces the value of $\cos\beta$ has to be corrected by

multiplication by a factor −1. This correction has been applied to the top half of the data displayed in Figure 4.5 (and in the analogous figures discussed later in the text).

The close-up panels of Figure 4.5 show that the 8CB molecules at the interface with the (001) molybdenite surface have a planar alignment, corresponding to an intense peak at around $\cos\beta \approx 0$. The different orientation of 8CB molecules also affects the density of the sample. For instance, the intense peak of the density observed in Figure 4.4 can be ascribed to 8CB molecules closely packed parallel to the surface.

Above the interface the 8CB molecules tend to align their alkyl chain toward the molybdenite surface, as shown by the peak at positive values of $\cos\beta$. In this region the 8CB molecules present a tilt angle of about 14.5° w.r.t. the surface, in good agreement with the experimental determinations reporting an anchoring angle of ±17.5° [24]. This induced alignment appears to propagate in the region up to 10 Å above the molybdenite surface, after which the distribution of orientations becomes isotropic.

Order Parameters

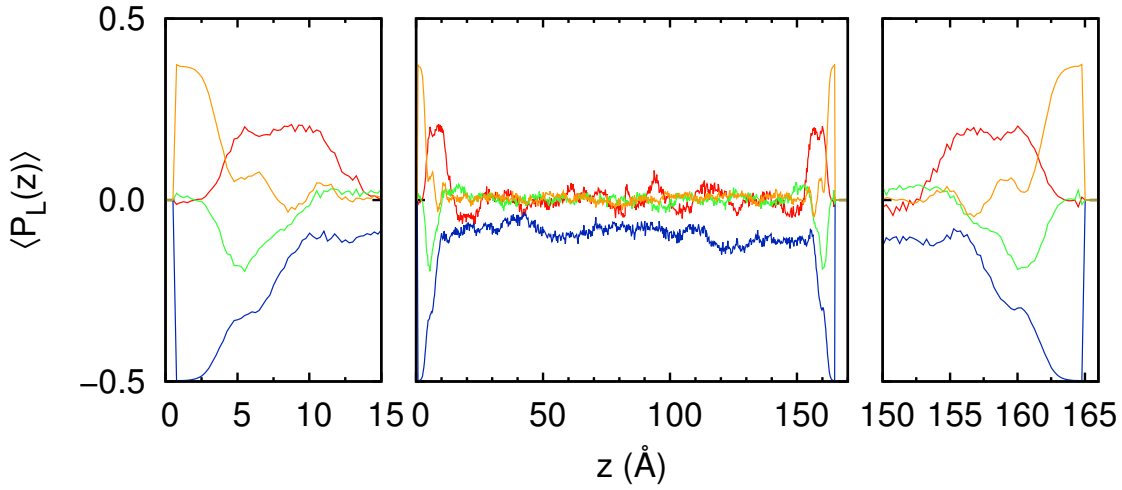

Figure 4.6: Order parameters ($\langle P_1\rangle$ red, $\langle P_2\rangle$ blue, $\langle P_3\rangle$ green, $\langle P_4\rangle$ orange) of the 8CB film at 325 K across the film (middle) and close to the interface with the surface (left and right), computed with respect to the normal at the surface z.

The polar order parameters computed with respect to the normal to the surface z provide evidence about the molecular organization within the sample. A plot of the order parameters from rank 1 to rank 4 is shown in Figure 4.6. At the two interfaces, the value of $\langle P_2(z)\rangle$ is close to -0.5, corresponding to molecules oriented planar to the surface. As the value of $\langle P_2(z)\rangle$ increases going toward the centre of the film, the $\langle P_1(z)\rangle$ value becomes positive, corresponding to molecules with their alkyl chains oriented toward the molybdenite surface. We also observe a non-zero value of $\langle P_3(z)\rangle$ at the interfaces. This parameter determines the average nonlinear susceptibility tensor element χ^2_{zzz}, which can be measured with the Surface Second Harmonic Generation (SHG) spectroscopy[1] [7, 57, 62].

[1]The SHG spectroscopy is based on a non-linear optic phenomenon where two photons interacting with a material give a new photon with twice the frequency of the initial photons [62]. SGH spectroscopy provides information about the electronic structure, atomic organization and molecular orientation of molecules in close contact with the surface (the technique applies to the first 2 or 3 monolayers) [62, 59].

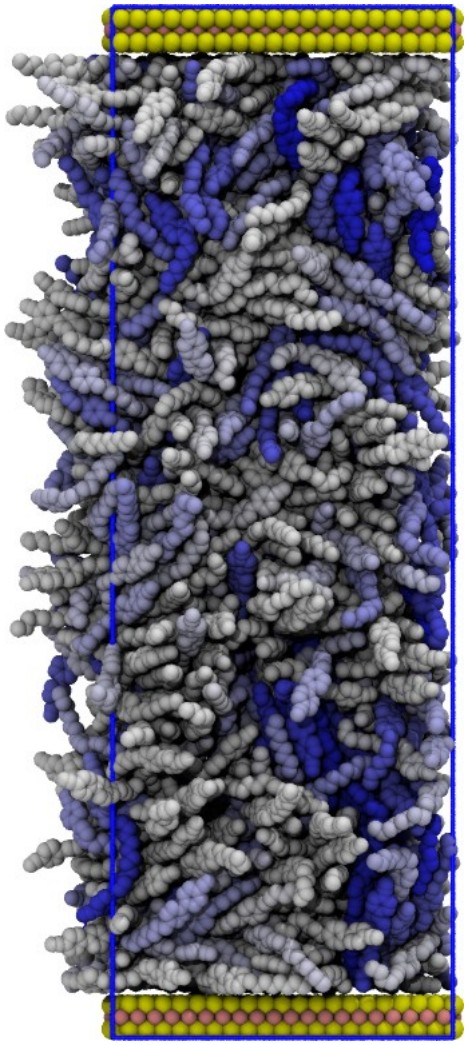

Figure 4.7: Snapshot of the 8CB sample in its isotropic phase. The colour of the molecules corresponds to their orientation: planar (white), homeotropic (blue).

The $\langle P_3(z)\rangle$ parameter in non-zero in a very thin layer close to the interface. We observe a similar behaviour for the $\langle P_4(z)\rangle$ parameter, which could be theoretically determined using depolarized Raman or fluorescence depolarization experiments. To the best of our knowledge these experimental determinations have not been carried out. We hope with this work to stimulate new experimental investigations on this system, which will benefit from the theoretical framework provided by the knowledge of the order parameters at the interface.

A computer-generated model of the 8CB film at 325 K is presented in Figure 4.7. The molecules displayed in Figure 4.7 are coloured according to their orientation. The first layer of 8CB molecules is planar, then the second layer is tilted from a few (on the left) to 90 degrees (on the right). This phenomenon is observed at both interfaces, confirming that the isotropic phase is well equilibrated, since the results obtained are symmetric. The *bulk-like* part of the sample is isotropic, even if it seems here that the planar orientation (white) is predominant.

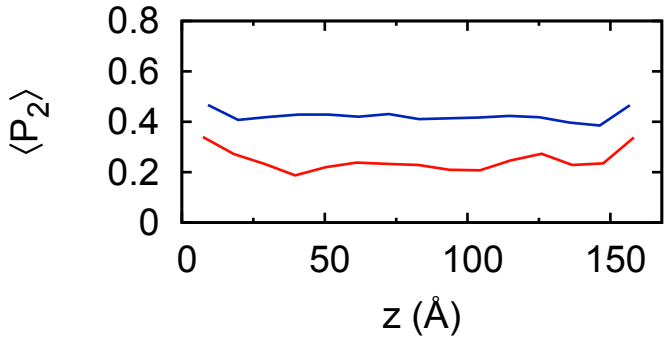

Figure 4.8: Scalar order parameter $\langle P_2 \rangle$ of 8CB film at 325 K (red, isotropic phase) and at 310 K (blue, nematic phase), computed in different layers along the normal at the surface z.

Important additional informations can be obtained from the scalar order parameter $\langle P_2 \rangle$, which express the local ordering of molecules with respect to the average director $\mathbf{n}(z)$, computed in discrete layers of 10 Å. The data shown in Figure 4.8 are computed for the nematic and isotropic phases of 8CB, which differ for the different value of $\langle P_2 \rangle$. An interesting result is that the molybdenite surface increases the local order of 8CB molecules. This effect is more evident in the isotropic phase, where it propagates up to two layers, than in the nematic phase, where it propagates only in the first layer.

4.3.2 Nematic phase

The nematic phase of 8CB was simulated for a total period of 210 ns, as shown in Figure 4.3, of which the production time corresponds to the last 100 ns of the MD trajectory.

Density Profile

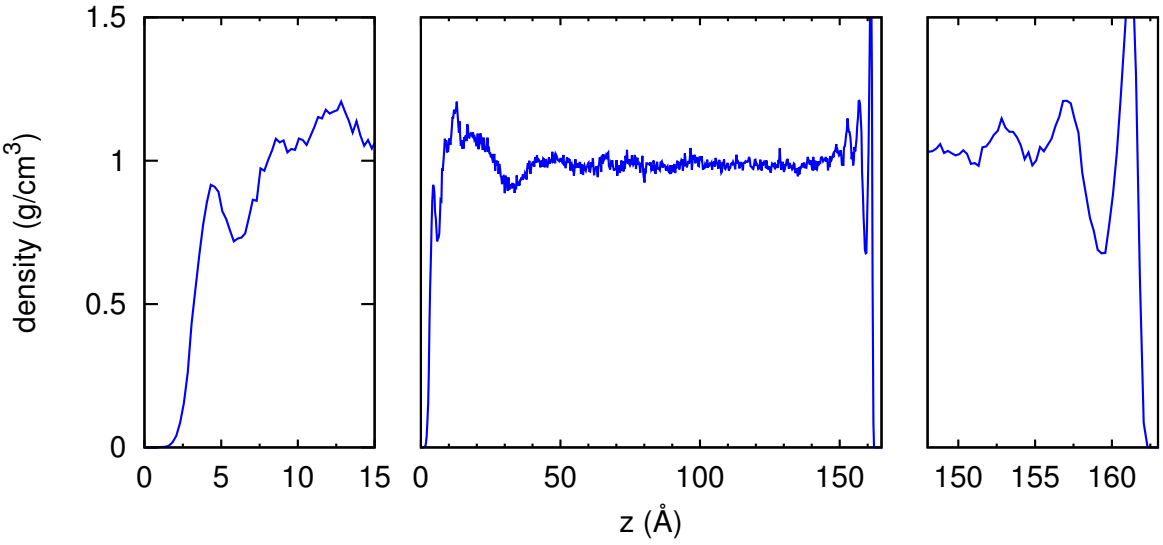

Figure 4.9: Density $\rho(z)$ of 8CB at 310 K across the film (middle panel) and at the interfaces (left and right panels), with respect to the normal at the surface z.

The computed density $\rho(z)$ of 8CB (Figure 4.9) is uniform across the bulk and similar to that of the isotropic phase. However, the two interfaces with the molybdenite present a different profile. On the left interface, a small peak is followed by two broad peaks with density slightly higher than that of the bulk. On the right interface we observe a narrow and intense peak, followed by three similar peaks with decreasing intensity. The difference between the two interfaces is due to a different organisation of the 8CB molecules, which in turn can be ascribed to a molecular reorganisation of the entire sample. In order to confirm this interpretation, we are currently carrying out new MD simulations to extend the simulated nematic phase for further 100 ns. The results of the new simulations will be discussed in a future scientific work.

Orientation of Molecules

An insight about the molecular organisation of 8CB molecules at the two interfaces is given by the orientational-positional distribution function $P(z, \cos\beta)$ map, displayed in Figure 4.10. The left interface observed in Figure 4.9 corresponds to the lower interface in Figure 4.10. The small peak at $z \sim 0$ corresponds to molecules aligned planar w.r.t. the surface. As observed in the isotropic phase, this peak is followed by a region where the molecules align their alkyl chains toward the surface, giving positive values of $\cos\beta$. In the nematic phase this peak eventually result in a peak at $\cos\beta = 1$, corresponding to molecules aligned vertically. This peak is followed by another one at $\cos\beta = -1$, corresponding to molecules pointing their cyano groups anti-parallel to the previous molecules. The resulting configuration is homeotropic and it is analogous to the interface formed by nCB molecules at the interface with vacuum [43, 49].

The right interface is characterised by an intense peak at $\cos\beta \sim 0$, corresponding to a planar orientation. This peak is followed by other peaks around the same orientation, but biased toward positive values of $\cos\beta$. We also observe an asymmetry of the probability map, which may indicate the formation of a layer of molecules oriented homeotropically w.r.t. the surface.

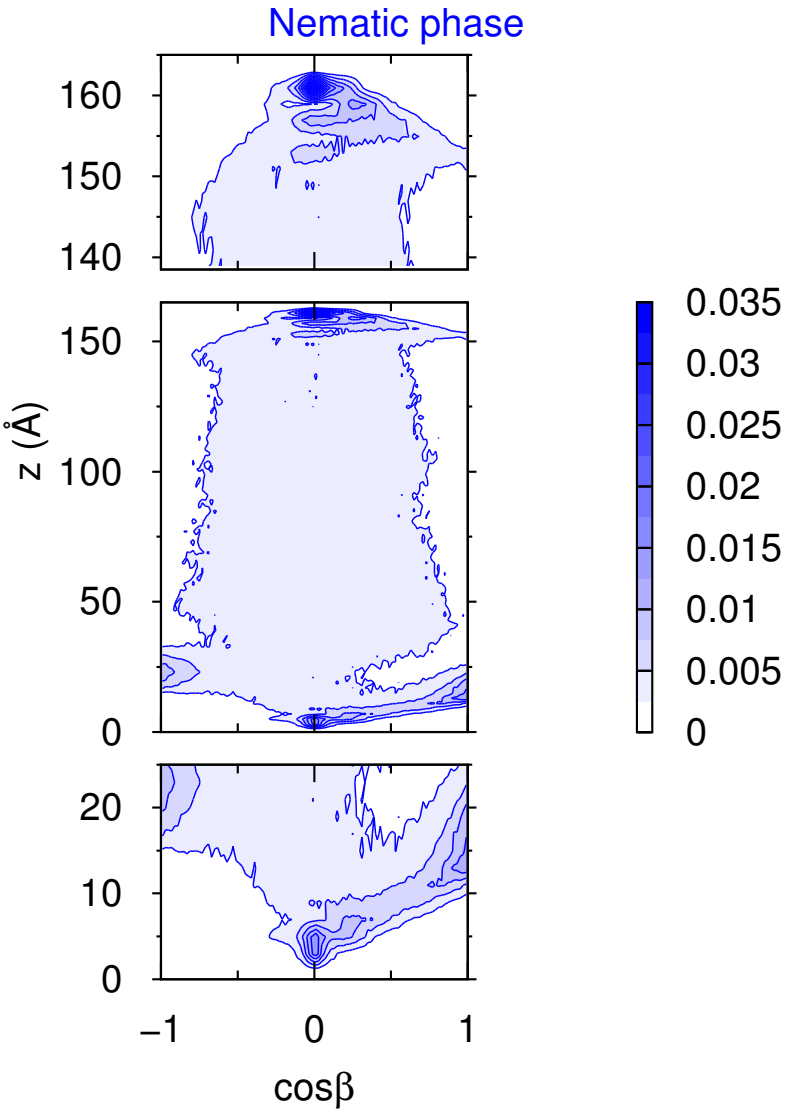

Figure 4.10: Blue-shaded contour map of the probability distribution $P(z, \cos\beta)$ of the 8CB film at 310 K. The top and bottom panels show a close-up of the function at the 8CB/MoS_2 interface.

Order Parameters

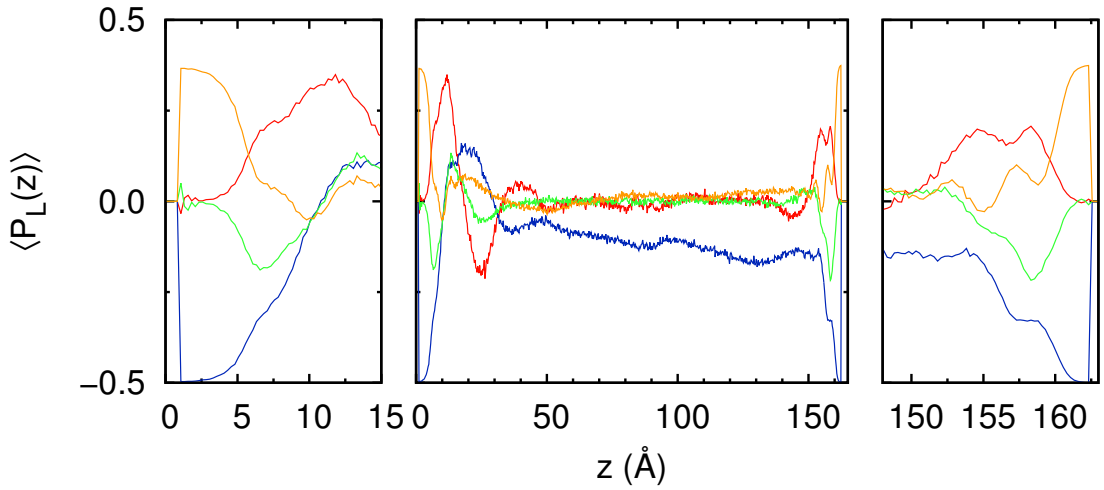

Figure 4.11: Order parameters ($\langle P_1 \rangle$ red, $\langle P_2 \rangle$ blue, $\langle P_3 \rangle$ green, $\langle P_4 \rangle$ orange) of the 8CB film at 310 K across the film (middle) and close to the interface with the surface (left and right), computed with respect to the normal at the surface z.

The asymmetry between the two interfaces of 8CB discussed in the previous section is reflected in the values of the order parameters. The $\langle P_1(z) \rangle$ parameter is zero at both interfaces, and then it goes toward positive values, confirming the tendency of 8CB molecules to point their alkyl chains toward the molybdenite surface. On the left interface, the double layer of molecules oriented homeotropically is reflected by a positive and negative peak of the value of $\langle P_1(z) \rangle$, while at the right interface only a positive peak is observed. The main difference between the two surfaces can be quantified by looking at the value of $\langle P_2(z) \rangle$, which varies continuously throughout the sample.

From these profiles it can be concluded that although the nematic phase is formed (which is also confirmed by the local value of the scalar order parameter $\langle P_2 \rangle$, reported in Figure 4.8), the 8CB film is undergoing a structural change at the scale length of the entire sample.

A snapshot of the 8CB film at 310 K is displayed in figure 4.12.

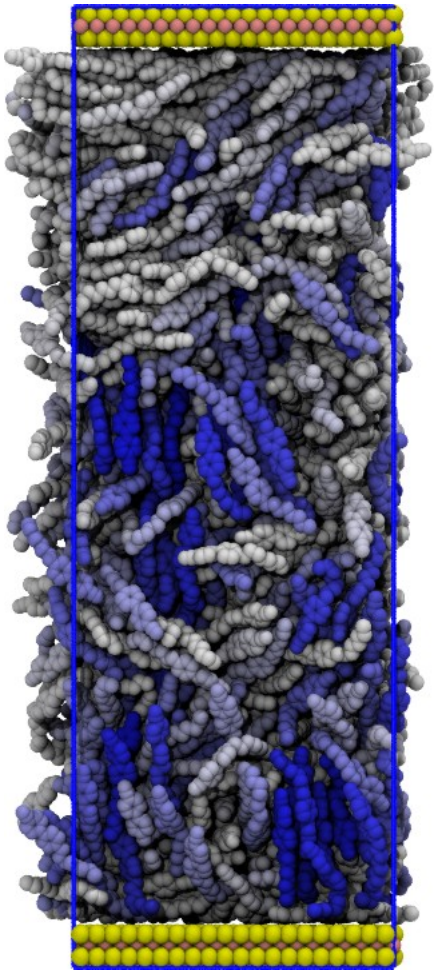

Figure 4.12: Snapshot of the 8CB sample in its nematic phase. The color of the molecules corresponds to its orientation: planar (white), homeotropic (blue).

The layer of 8CB molecules in a planar configuration and the over-layer of molecules oriented homeotropically is clearly visible at the bottom surface in Figure 4.12. Small clusters of molecules sharing the same orientation are visible, scattered across the film. Conversely, the 8CB molecules on the top surface maintain a planar orientation.

Chapter 5

Computer simulations of 7CB on MoS_2

5.1 Introduction

The class of nCB LCs present fluctuations of their physical properties which depend on the number of carbon atoms in their alkyl chains. This effect is referred to as *odd-even* effect, and it has also been observed in the formation of different patterns for nCB adsorbed on (001) MoS_2 surfaces [24].

In this chapter we study the orientation and morphology of a thin film of 7CB on the (001) molybdenite surface, paying particular attention to the comparison between the results presented here and those discussed in the previous chapter.

5.2 Computational details

MD simulations of the 7CB/MoS_2 system were carried out in the NPT ensemble, using a Langevin barostat to control the pressure and the temperature. The sample studied here is composed of 1000 7CB molecules and a slab of molybdenite which has the same characteristic of that discussed in the previous chapter. The isotropic phase of 7CB was simulated at 325 K, while the nematic phase was formed by cooling the sample at 315 K.

5.3 Results and Discussion

5.3.1 Isotropic phase

The energy of the 7CB sample at 325 K (isotropic phase) and 315 K (nematic phase) is reported in Figure 5.1.

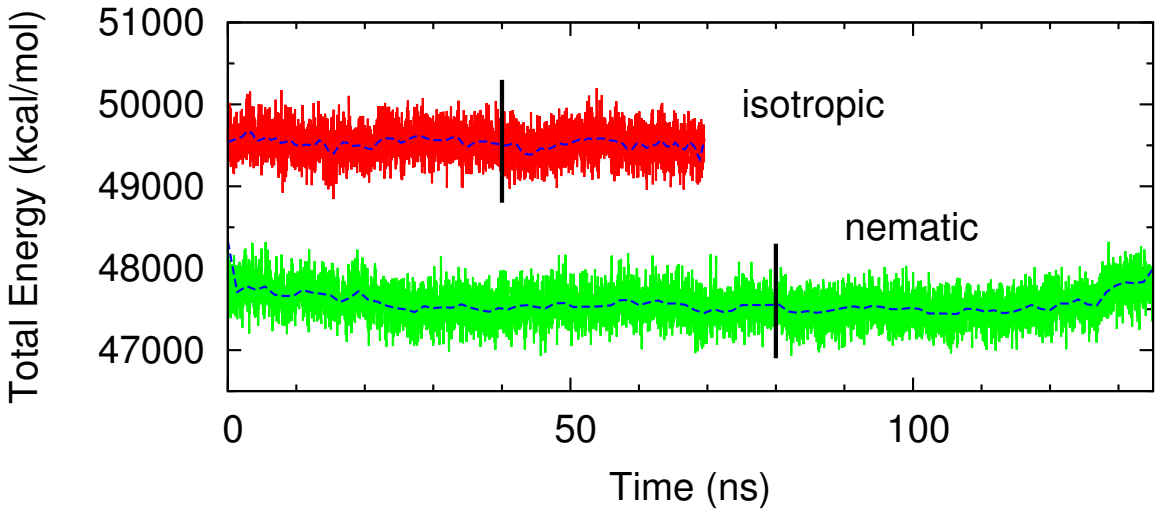

Figure 5.1: Total energy of the 7CB/MoS_2 system at 325 K (red line, isotropic phase of 8CB) and at 315 K (green line, nematic phase). Dashed lines show the mean value of energy, while the vertical black lines mark the beginning of the production phase in each MD trajectory.

For the isotropic phase, roughly 40 ns were necessary to achieve thermal equilibrium. Although the MD simulation of the nematic phase discussed here spans for 135 ns, it appears not to be at thermal equilibrium. However, we will present a preliminary analysis of the molecular orientation of 7CB at 315 K carried out in the last 45 ns of the simulated trajectory.

Density Profile

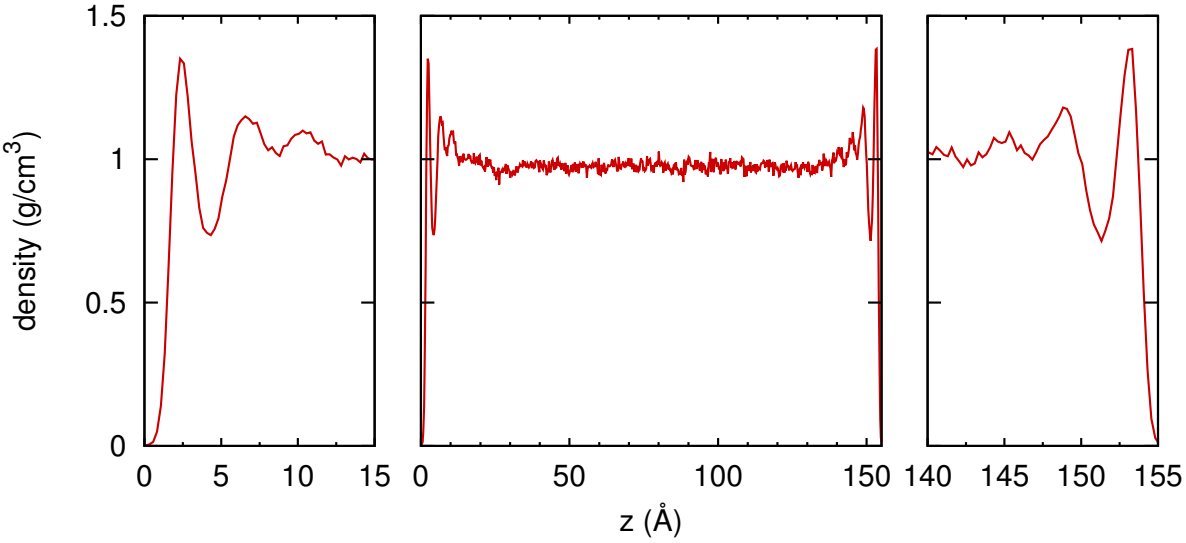

Figure 5.2: Density $\rho(z)$ of 7CB at 325 K across the film (middle panel) and at the interfaces (left and right panels), with respect to the normal at the surface z.

The density $\rho(z)$ of 7CB computed at 325 K is shown in Figure 5.2. The two 7CB/MoS_2 interfaces appear to be similar, having the same kind of fluctuations already seen for the

isotropic phase of 8CB. Conversely, the density is uniform across the bulk, providing evidence that the thermal equilibrium is reached.

Orientation of Molecules

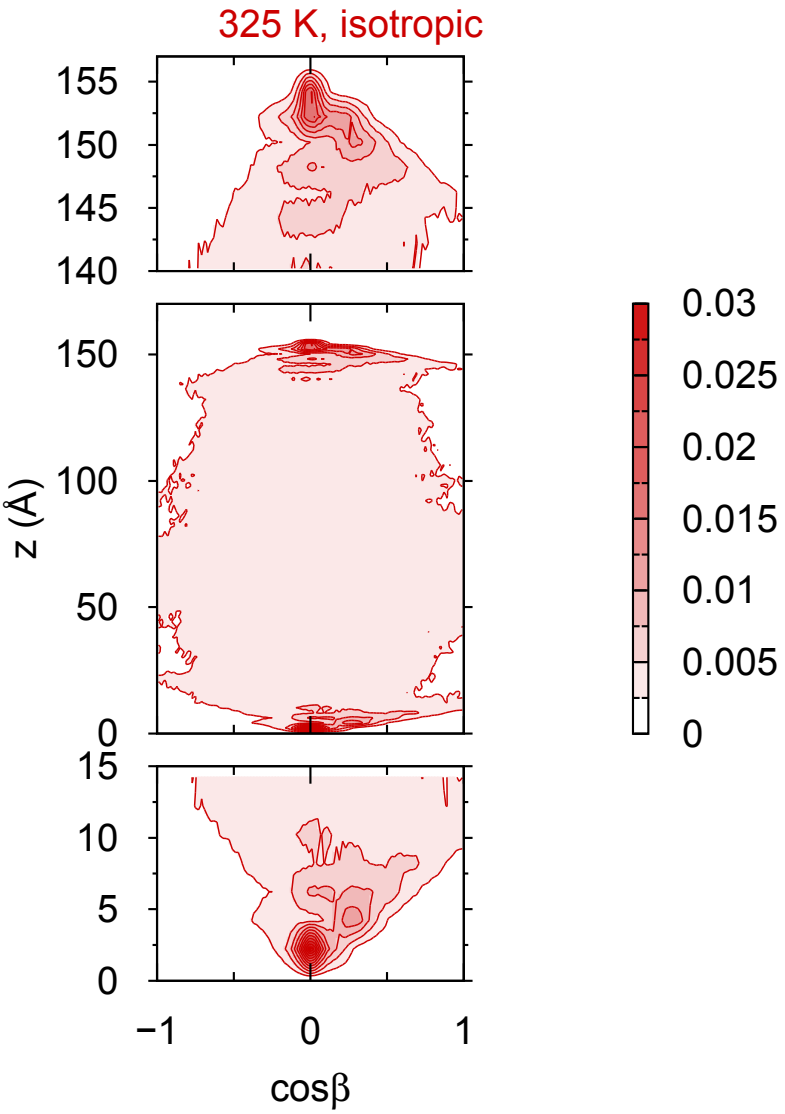

Figure 5.3: Red-shaded contour map of the probability distribution $P(z, \cos\beta)$ of the 7CB film at 325 K. The top and bottom panels show a close-up of the function at the 7CB/MoS_2 interface.

The orientational-positional distribution function $P(z, \cos\beta)$ map of 7CB at 325 K is displayed in Figure 5.3. The orientation of 7CB molecules at the interface with molybdenite appears to be planar, as shown by the two intense peaks at $\cos\beta = 0$. The first over-layer of 7CB molecules are oriented with their alkyl chains pointing toward the surface of molybdenite, forming a tilt angle of about 11°. The effect of the surface is confined to the first 10 Å of the 7CB sample, after which an isotropic distribution of orientations is established.

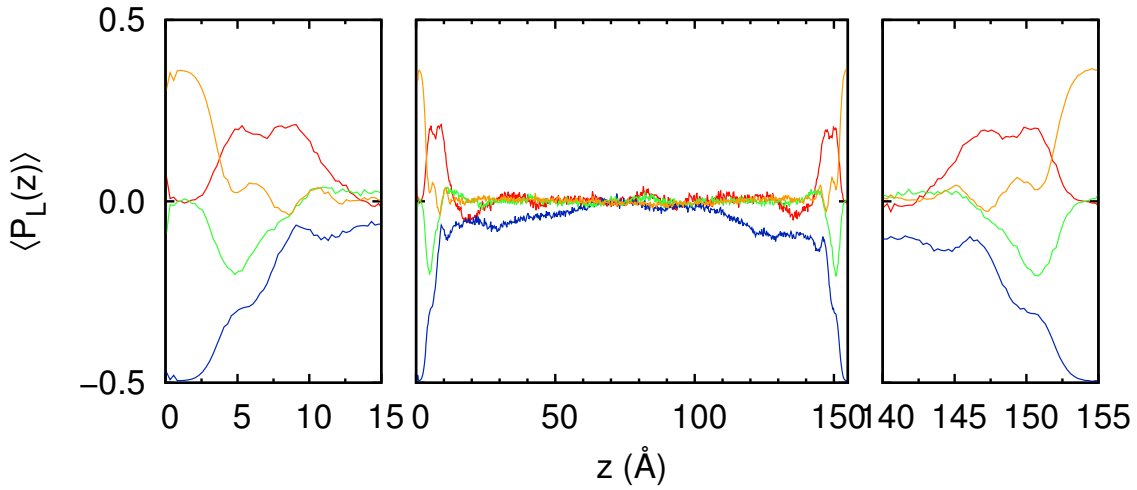

Figure 5.4: Order parameters ($\langle P_1 \rangle$ red, $\langle P_2 \rangle$ blue, $\langle P_3 \rangle$ green, $\langle P_4 \rangle$ orange) of the 7CB film at 325 K across the film (middle) and close to the interface with the surface (left and right), computed with respect to the normal at the surface z.

At the two interfaces, the value of $\langle P_2(z) \rangle$ is close to -0.5, corresponding to molecules oriented almost planar to the surface. As the value of $\langle P_2(z) \rangle$ increases going toward the centre of the film, the $\langle P_1(z) \rangle$ value becomes positive, corresponding to molecules with their alkyl chains oriented toward the molybdenite surface.
We also observe a non-zero value of $\langle P_3(z) \rangle$ in a thin region close to the interface. The $\langle P_4(z) \rangle$ parameter also displays a similar behaviour.

A computer-generated model of the 7CB film at 325 K is presented in Figure 5.5.

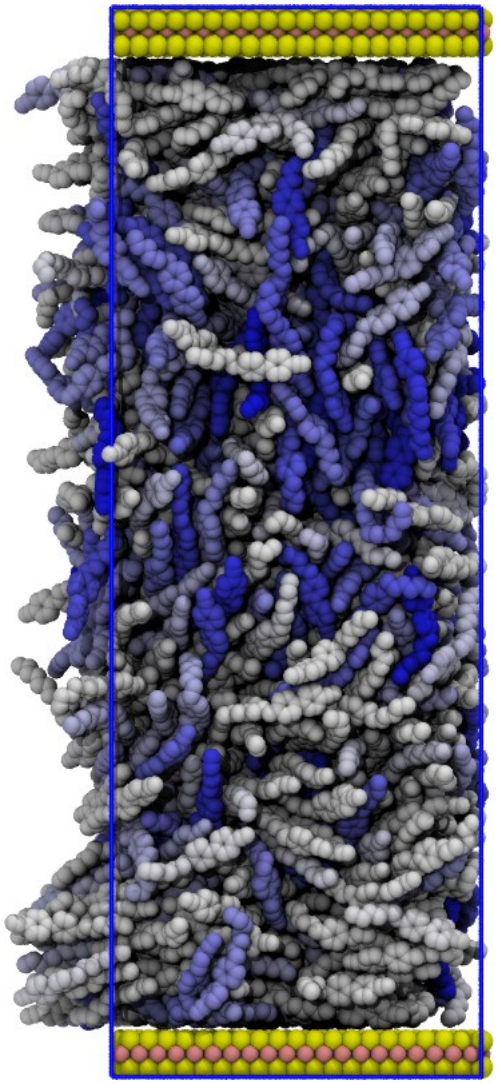

Figure 5.5: Snapshot of the 7CB sample in its isotropic phase. The colour of the molecules corresponds to their orientation: planar (white), homeotropic (blue).

The molecules displayed in Figure 5.5 are coloured according to their orientation. The 7CB molecules in the layer in contact with the molybdenite surface are in a planar configuration, while then the molecules in the second layer are slightly tilted. This phenomenon is observed at both interfaces, confirming that the isotropic phase is well equilibrated, since the results obtained are symmetric. The central part of the sample is isotropic and it is characterised by molecules arranged in random configurations.

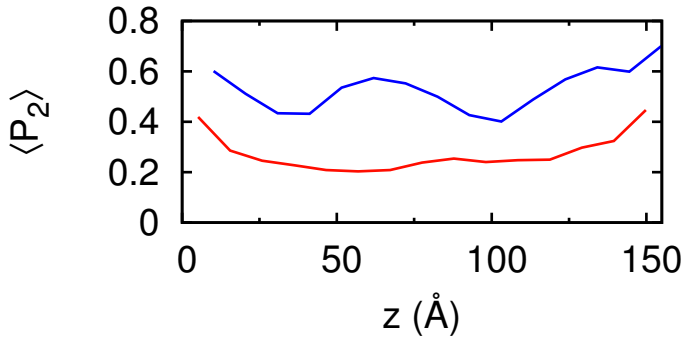

Figure 5.6: Scalar order parameter $\langle P_2 \rangle$ of 7CB film at 325 K (red, isotropic phase) and at 315 K (blue, nematic phase), computed in different layers along the normal at the surface z.

The scalar order parameter $\langle P_2 \rangle$ computed in discrete layers of 10 Å is shown in Figure 5.6. The $\langle P_2 \rangle$ parameter computed for isotropic phase of 7CB shows is constant throughout the sample and increases at the interface with molybdenite. The same behaviour is observed for the nematic phase. However, the variations of the $\langle P_2 \rangle$ parameter in the central part of the 7CB film suggest that the nematic phase is not yet formed.

5.3.2 Nematic phase

Density Profile

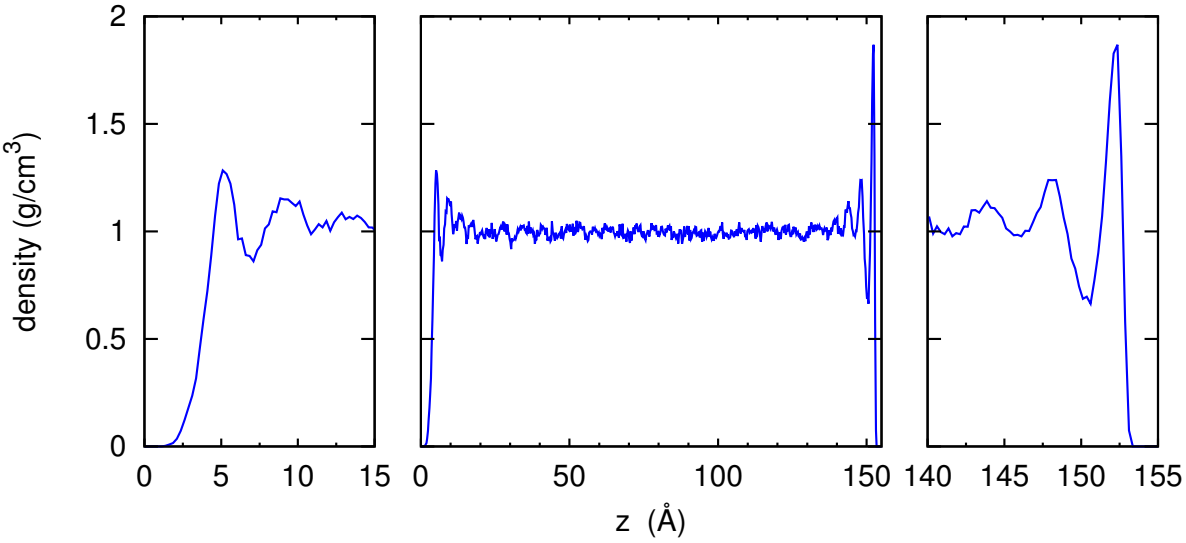

Figure 5.7: Density $\rho(z)$ of 7CB at 315 K across the film (middle panel) and at the interfaces (left and right panels), with respect to the normal at the surface z.

The computed density $\rho(z)$ of 7CB (Figure 5.7) is uniform across the bulk and similar to that of the isotropic phase. However, the two interfaces with the molybdenite present a slightly different profile. On the left interface, the oscillations of the density are more damped that those on the right interface. However, the frequency of oscillations in both interfaces is similar, suggesting that both sides of the film are oriented in the same way. In order to confirm this interpretation, we are currently carrying out new MD simulations to extend

the simulated nematic phase for further 100 ns. The results of the new simulations will be discussed in a future scientific work.

Orientation of Molecules

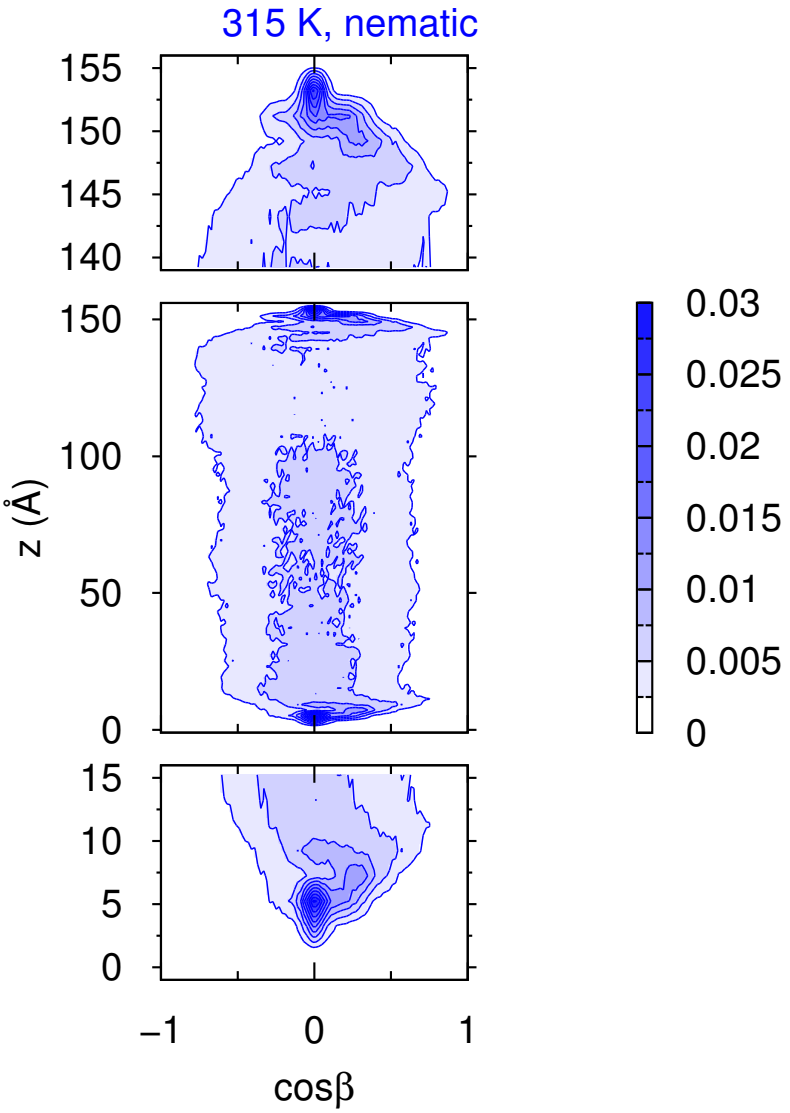

Figure 5.8: Blue-shaded contour map of the probability distribution $P(z, \cos\beta)$ of the 7CB film at 315 K. The top and bottom panels show a close-up of the function at the 7CB/MoS_2 interface.

An insight about the molecular organisation of 7CB molecules at the two interfaces is given by the orientational-positional distribution function $P(z, \cos\beta)$ map, displayed in Figure 5.8. The left interface observed in Figure 5.7 corresponds to the lower interface in Figure 5.8. The peak at $z \sim 0$ corresponds to molecules aligned planar w.r.t. the surface. This peak is then followed by a region where the molecules align their alkyl chains toward the surface, giving positive values of $\cos\beta$. Unlike the nematic phase of the 8CB, the molecules of 7CB do not form a second layer of molecules aligned vertically. Instead, a planar orientation is established in the central part of the film, even though the noise observed in the central part

of the map appears to be correlated with the low value of the scalar order parameter $\langle P_2 \rangle$ (see Figure 5.6).

Order Parameters

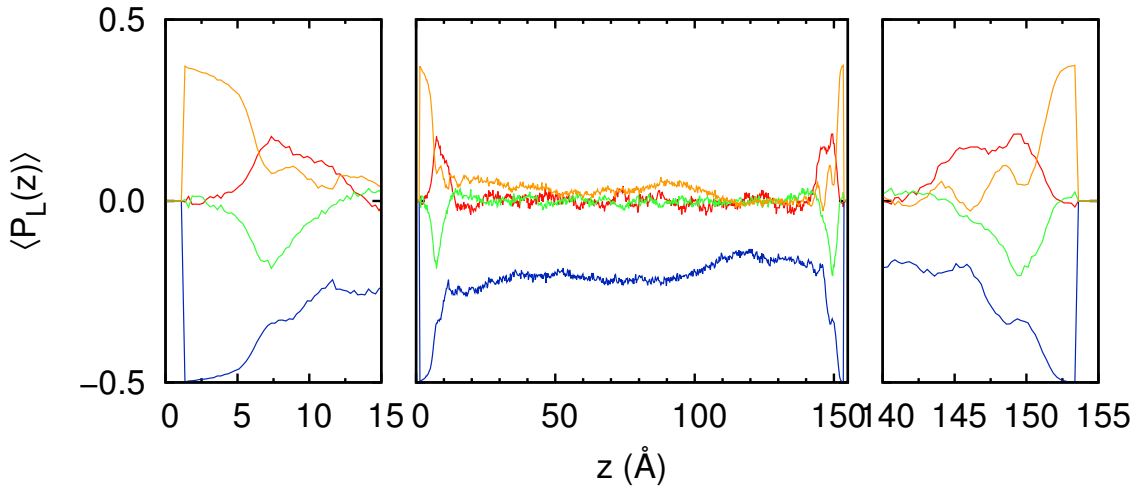

Figure 5.9: Order parameters ($\langle P_1 \rangle$ red, $\langle P_2 \rangle$ blue, $\langle P_3 \rangle$ green, $\langle P_4 \rangle$ orange) of the 7CB film at 315 K across the film (middle) and close to the interface with the surface (left and right), computed with respect to the normal at the surface z.

The order parameter $\langle P_1(z) \rangle$ is zero at both interfaces, and then it goes toward positive values, confirming the tendency of 7CB molecules to point their alkyl chains toward the molybdenite surface. Interestingly, the parameter $\langle P_2(z) \rangle$ has a value of -0.5 at the two interfaces, corresponding to planar orientation, and keeps negative values throughout the entire sample. Although the influence of the surface appears to be stronger in a small region above the interface, the planar orientation extends to all molecules in the 7CB film. In the region at around 110 Å into the sample, the parameter $\langle P_2(z) \rangle$ has values less negative than in the rest of the film. This change is correlated with the broad distribution of orientations displayed in the same region in figure 5.8.

From these profiles it can be concluded that although the nematic phase is formed, the 7CB film is undergoing a structural change at the scale length of the entire sample.

A snapshot of the 7CB film at 315 K is shown in Figure 5.10.

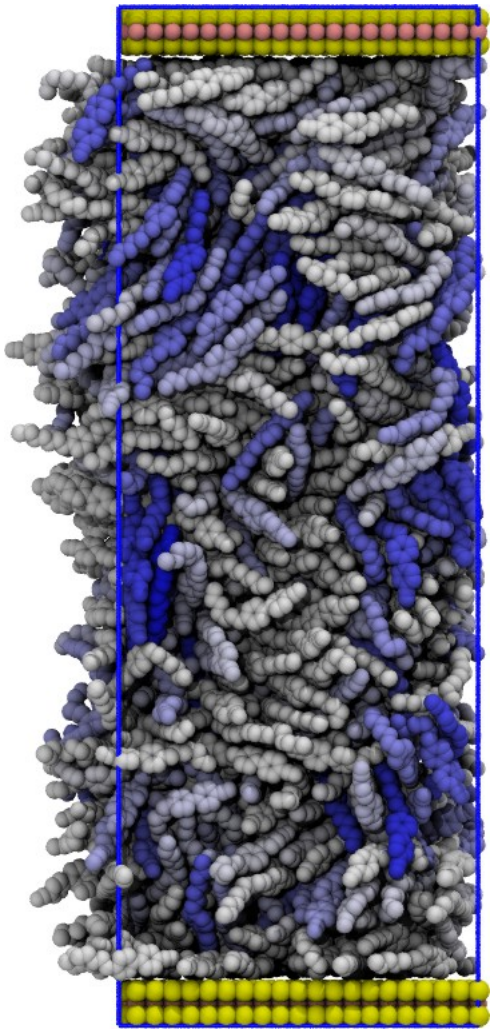

Figure 5.10: Snapshot of the 7CB sample in its nematic phase. The color of the molecules corresponds to its orientation: planar (white), homeotropic (blue).

A layer of 7CB molecules in a planar configuration is visible at both interfaces. Also, a significant part of the sample is characterised by molecules in a planar orientation, even if small clusters of molecules with a vertical orientation are present.

Chapter 6

Conclusions and future work

We presented MD simulations of two films of liquid crystals supported on (001) MoS_2 surfaces. We developed a force field to model the interactions between the LC molecules and the molybdenite surface by fitting absorpion energy curves of one molecule of 7CB on molybdenite computed at the DFT level of theory. The two LC studied (7CB and 8CB) belong to the class of the n-alkyl-4' cyanobiphenyl compounds(nCB, where n indicates the number of carbon atoms in the alkyl chain) and have been modelled with a force field previously optimized to accurately reproduce a large number of physical properties of this class of molecules [51].

The analysis of the MD simulations reveals that a planar orientation is established at the interface between the LC and the solid substrate. Significant differences have been observed between the orientation of the 7CB and 8CB across the film, while for the isotropic phase a planar orientation is found at the interface. The influence of the molybdenite surface onto the LC films appears to be limited in the first 15 Å above the interface. Overall, the results obtained are in agreement with the experimental determinations carried out by Lacaze et al [25, 24, 26, 27].

A summary of the structural findings presented in this thesis follows:

- The (001) surface of MoS_2 increases the order of nCB molecules in either the isotropic and nematic phases.
- A planar configuration is found to be the most energetically stable at the interface with the solid substrate.
- The effect of the surface is confined to a region of about 15 Å above the interface.
- The simulated anchoring angle of the 8CB on the surface was 14.5° w.r.t. the surface, in good agreement with experimental value of 17.5° [27].

Despite the fact that the MD simulations of the nematic phases of both 7CB and 8CB extended for over 100 ns, we found that the nematic phases were not fully equilibrated. As a future work, we propose to extend the current range of MD simulations.

Acknowledgements

I would like to express my gratitude to Professor Zannoni for accepting me as a Master student in his lab, and for his expert advices and supervision during this master thesis work, his patience and his kindness. His teaching skills and methods are a real inspiration, and I will keep him as a model in the future, when it will be my turn to teach.
I want to thank also post-doctoral fellow Dr. Otello Roscioni, who accompanied me during this work, providing help and resources, as well as many advices. He was comprehensive about my needs and demands, and brought me a lot. I am confident he will be a great teacher in the future.
I would like to award a special thank to my room-mate Gabriel, for his support during this work, as well as to Diandian Wang, another student of the ASC master for all the discussions, coffee breaks, and everything we did together that made the thesis writing more easier and pleasant.
To all the teachers that I had the pleasure to be the student of during theses two years of master, thank you. I learned a lot, and particularly enjoyed the way you transmitted us your knowledges. The courses were diverse and interesting.
I want to thank Professor Cristol, the ASC master headmaster, and Professor Righi, the local coordinator, for their patience, help and advices during theses two very important years.
Thank you to all the staff in Professor Zannoni's lab for welcoming me warmly.
And thank you to all the people that I did not mention that helped me at one moment or another.

Alexandre Samuel Dumon
July 15, 2013

Appendix A

X-Ray Diffraction

The work of E. Lacaze et al. uses X-ray diffraction (XRD) to gain information about the structure of the anchoring of 8CB on the surface. Here, we will outline the basis of this experimental technique, referring to most advanced textbooks for more detailed explanations.
X-Ray diffraction (XRD) is a not a typical spectroscopic technique. Indeed, spectroscopic techniques correspond to the measure of the absorption of a probing beam by a sample. In the case of XRD, we actually observe the diffraction of the X-rays by the electronic cloud of atoms and molecules, so, etymologically speaking, XRD is not a spectroscopy method, but rather a spectrometry method.
X-Ray Diffraction is a technique relying on the diffraction of X-rays by the electronic clouds in a regular shaped structure (crystal) [19]. The basic law of XRD is the Bragg law [19]:

$$2dsin(\theta) = n\lambda \tag{A.1}$$

This law can be easily determined using the following scheme:

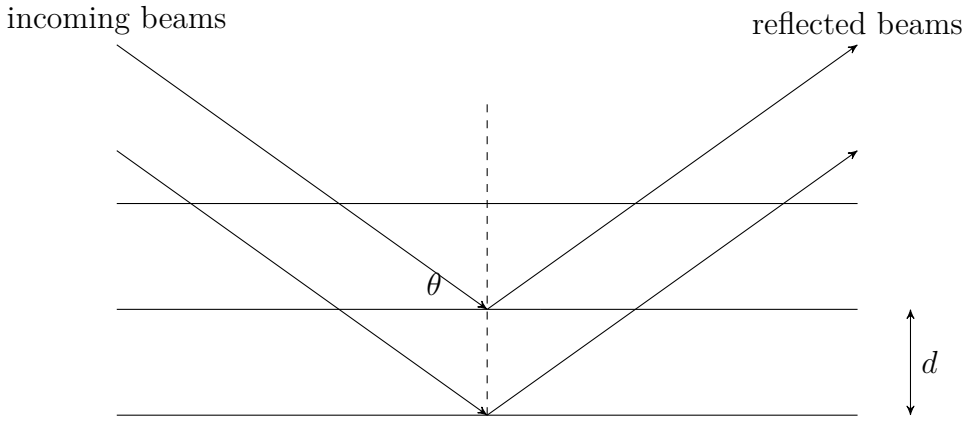

Figure A.1: Bragg law scheme

This law represents the conditions to have reflection by an atomic plan. In Figure A.1, d is the interplanar distance, θ the incidence angle, λ the wavelength of the incoming wave, and n an integer. If this condition is not met, we will observe no reflection.
They are 219 space groups for a crystal, all of them have their own particular features: geometry, atom position, symmetry axis, fold axis [19]. Theses geometries belong to 32 different space groups. The next two figures shows two of them:

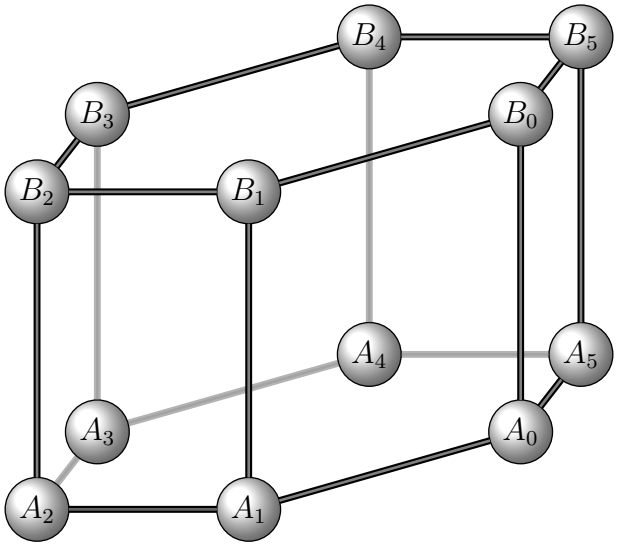

Figure A.2: hexagonal structure P_{6_3} mmc (these of MoS_2

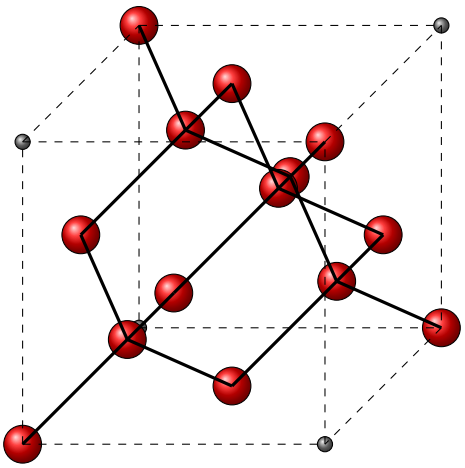

Figure A.3: diamond structure: F d 3 m (face centered cubic)

As mentioned earlier, XRD is a spectrometry method, but it also present another interesting feature. The scattered intensity, $I(k) \propto |E(k)|^2$, where $E(k) \propto \int \rho(r) e^{i(k.r)} dr$ is the Fourier transform of the electron density [19]. But, because of the square, we cannot recover the electron density (and therefore the structure) from the scattered intensity. The solution is to work the other way round. Since they are a not a lot of geometric solutions, from the hypothetic structure we can simulate the hypothetic spectrum, and see if it matches the experimental spectrum. Moreover, the existence of databases, and the increase of the computer power make this kind of method easier every day [19].
A typical XRD spectrum is displayed in the next figure:

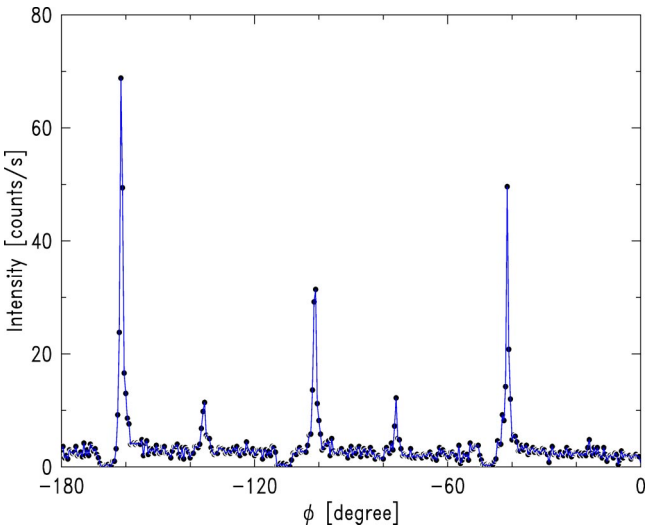

Figure A.4: XRD spectrum of 8CB on a molybdenite surface

Remaining the way of producing the X-rays. Electrons a produced (usually by heating a tungsten wire), and then go hit a cooled metallic target (usually molybdenum), that will emit then X-rays according to the following scheme [19]:

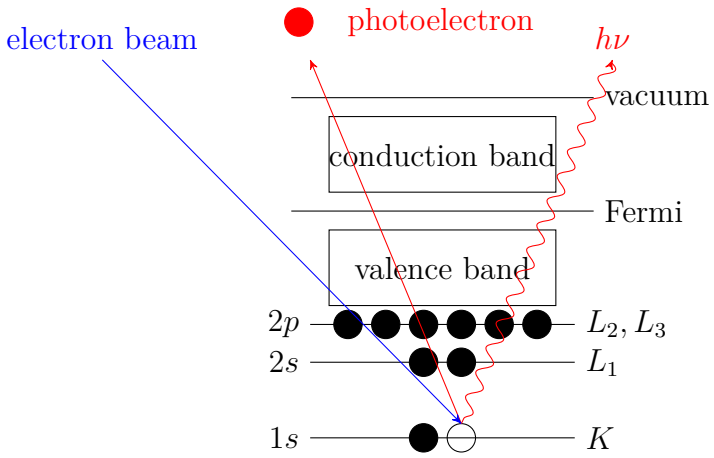

Figure A.5: X-rays production

The wavelength of the X-rays depends on the target type, for example in the case of Molybdenum, there are a α and β emissions, and we usually get rid of the later one using a monochromator [19].

Appendix B

GULP

GULP is a program for performing a variety of simulations on materials using boundary conditions of 0-D (molecules and clusters), 1-D (polymers), 2-D (surfaces, slabs and grain boundaries), or 3-D (periodic solids) [15]. The focus of the code is on analytical solutions, through the use of lattice dynamics, where possible, rather than on molecular dynamics. A large number of force fields can be used with GULP, spanning from the shell model for ionic materials molecular mechanics for organic systems, the embedded atom model for metals and the reactive REBO potential for hydrocarbons. Analytic derivatives are included up to at least second order for most force fields, and to third order for many [15].
To make a calculation with GULP, we provide the software a file.gin, input file, that contains all the information required by the software to calculate what we need. The structure of this file is as following:

```
opti conp prop

# Created by GDIS version 0.90.0
#
#

switch bfgs gnorm 0.100000

name Becker

cell
3.1604 3.1604 12.2950  90.0000 90.0000 120.0000 1 1 1 0 0 0
fractional
Mo    core      0.333333     0.666666     0.250000      0.7600000
S1    core      0.333333     0.666666     0.629000     -0.3800000
S2    core      0.666667     0.333334     0.129000     -0.3800000
Mo    core      0.666667     0.333333     0.750000      0.7600000
S2    core      0.666666     0.333333     0.371000     -0.3800000
S1    core      0.333334     0.666667     0.871000     -0.3800000

species
Mo core    0.734
S  core   -0.367
end
```

```
morse
Mo core S  core 19.94  0.858  2.54 0.0 3.0
three
S  core Mo core Mo core  0.8968   81.67  0.0 4.0 0.0 4.0 0.0 8.0
Mo core S  core S  core  0.6356   81.78  0.0 4.0 0.0 4.0 0.0 8.0
lennard epsilon
Mo core  Mo core  1.5549  2.2310  0.0 15.0
Mo core  S  core  1.3802  2.9028  0.0 15.0
S1 core  S1 core  0.2981  3.0023  0.0 15.0
S2 core  S2 core  0.2981  3.0023  0.0 15.0
S1 core  S2 core  0.1656  3.0138  0.0 15.0

print 1
```

The first line contains different options specifying the conditions ('conp' for constant pressure), the kind of simulation (optimization of geometry ('opti')) and then what we want (prop will tell to the software to print the different properties in the output file).
We then provide the cell properties (a,b and c, α, β, γ. Additional digits are used to tell GULP whether to fit the corresponding parameter (1) or to do not (0).
The following lines provide the position of the species, and their charge.
The last step is provide the parameters that will allow GULP to calculate the different potential energies. Here the bounded interaction (two body) is calculated using a Morse curve, so we provide the dissociation energy (De), a, the parameter controlling the broadening of the curve, and r0 the equilibrium distance, the minimum radius and the maximum one. (as a reminding, a Morse potential is $\Phi_{Morse} = De * ((1 - exp^{a(r-r0)})^2 - 1))$.) The three body interaction is more tricky to understand. If the structure is A-B-C, we have to provide B A C to GULP, and he will know that B is the atom in the middle and so on. And the force is calculated as follow: $\Phi_{three-body} = \sum_{i=2}^{4} \frac{1}{i!} k_i(\theta - \theta_0)^i$. The k are in eV/rad, and corresponds to the energies of the bonds, $\theta 0$ is in rad, and is the equilibrium angle, the other digits are juste the minimum and maximum distance between the atoms.
The last part is the LJ interaction, that we provide by giving the r min, r max, epsilon and sigma for each interaction.
In the present case, this input file was for the relaxation of the structure of molybdenum (when we were trying to determine what was the best set of parameters, it will be detailed later), and since it presents 2 types of S (for the intra plane interactions, and the inter plane interactions), we denote them S1 and S2. Anywhere else, if the type does not matter (when we provide mass, charge, and all the required informations), we just use S. The option 'core' just specify that this atom belongs to the lattice.
After the calculation, GULP provides an output file named file.gout . It provides the energies (kinetic and potential), and everything that is required for an analysis of the data.

Appendix C

NAMD

NAMD is also a software for molecular dynamic, that is however more adapted to the simulation of big samples like proteins [39]. It indeed split the sample into residue, and then ask every processor of the cluster to calculate the energy for 1 or 2 residue type (it splits so the calculation between all the available processors), keeping one 'chief' processor, where all the other send their information, and that handle them, write the output file [39].
NAMD use a lot of different kind of files, with different formats, providing different kind of information. The next diagram shows the 'logic' structure of NAMD. The different types of files will be explained after this flowchart.

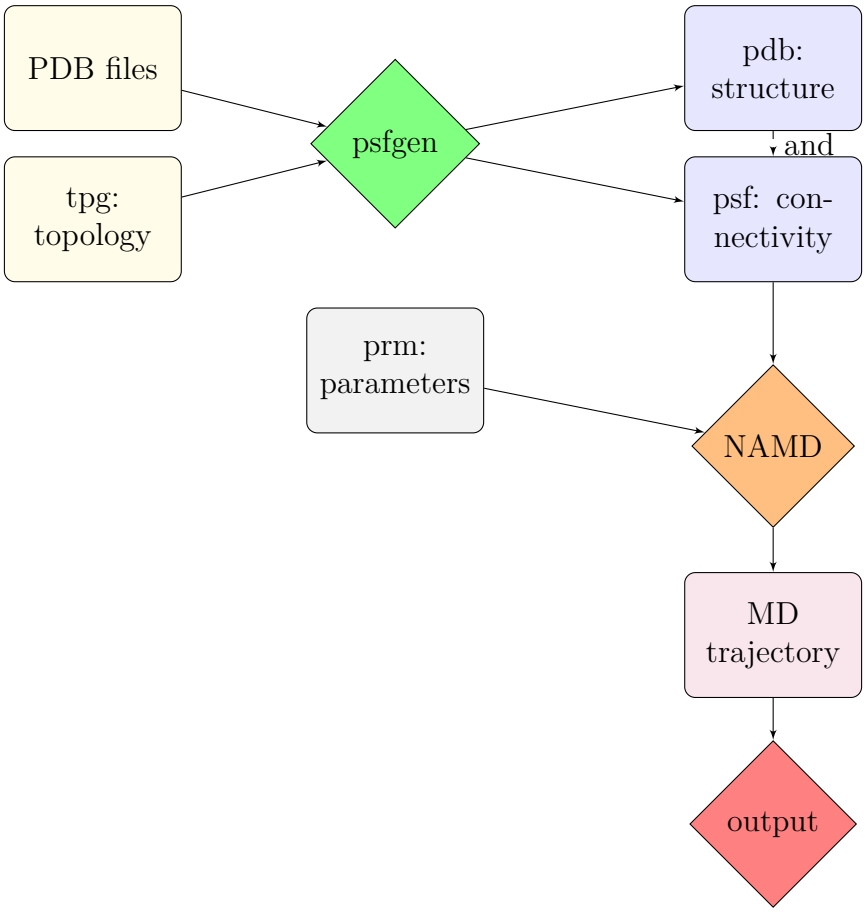

Figure C.1: Molecular dynamic calculations via NAMD structure

PDB stands for Protein DataBase, it contains the coordinates of the atoms, per residue (so here one pdb for the 7CB, one for the molybdenite) [39], the topology file contains the charges, the mass, and the bonds between atoms, as well as their name as residue (NAMD will then split them between the processor for calculation) [39]. We then use a program called psfgen that will generate the two files containing the total structure, and one with the connectivity, the masses. The file .prm is the parameter file, with the σ and ϵ, the angles of equilibrium, distance of equilibrium, for all the bounds. Those three files are our input files. Then NAMD calculate the trajectories, and provides us an output file, with the following structure.

```
Charm++: standalone mode (not using charmrun)
Converse/Charm++ Commit ID: v6.4.0-beta1-0-g5776d21
Charm++> scheduler running in netpoll mode.
CharmLB> Load balancer assumes all CPUs are same.
Charm++> Running on 1 unique compute nodes (2-way SMP).
Charm++> cpu topology info is gathered in 0.001 seconds.
Info: SIMULATION PARAMETERS:
Info: TIMESTEP                1
Info: NUMBER OF STEPS         0
Info: STEPS PER CYCLE         12
Info: PERIODIC CELL BASIS 1   59.44 0 0
Info: PERIODIC CELL BASIS 2   0 51.4766 0
Info: PERIODIC CELL BASIS 3   0 0 300
Info: PERIODIC CELL CENTER    0 0 0
Info: WRAPPING ALL CLUSTERS AROUND PERIODIC BOUNDARIES ON OUTPUT.
Info: LOAD BALANCER  Centralized
Info: LOAD BALANCING STRATEGY  New Load Balancers -- DEFAULT
Info: LDB PERIOD              2400 steps
Info: FIRST LDB TIMESTEP      60
Info: LAST LDB TIMESTEP      -1
Info: LDB BACKGROUND SCALING 1
Info: HOM BACKGROUND SCALING 1
Info: PME BACKGROUND SCALING 1
Info: MIN ATOMS PER PATCH     40
Info: INITIAL TEMPERATURE     300
Info: CENTER OF MASS MOVING INITIALLY? NO
Info: DIELECTRIC              1
Info: EXCLUDE                 SCALED ONE-FOUR
Info: 1-4 ELECTROSTATICS SCALED BY 0.833333
Info: MODIFIED 1-4 VDW PARAMETERS WILL BE USED
Info: SWITCHING ACTIVE
Info: SWITCHING ON            12
Info: SWITCHING OFF           15
Info: PAIRLIST DISTANCE       17.5
Info: PAIRLIST SHRINK RATE    0.01
Info: PAIRLIST GROW RATE      0.01
Info: PAIRLIST TRIGGER        0.3
Info: PAIRLISTS PER CYCLE     2
```

```
Info: PAIRLISTS ENABLED
Info: MARGIN                    0
Info: HYDROGEN GROUP CUTOFF  2.5
Info: PATCH DIMENSION          20
Info: ENERGY OUTPUT STEPS      12
Info: CROSSTERM ENERGY INCLUDED IN DIHEDRAL
Info: TIMING OUTPUT STEPS      120
Info: LANGEVIN DYNAMICS ACTIVE
Info: LANGEVIN TEMPERATURE    300
Info: LANGEVIN DAMPING COEFFICIENT IS 5 INVERSE PS
Info: LANGEVIN DYNAMICS APPLIED TO HYDROGENS
Info: PARTICLE MESH EWALD (PME) ACTIVE
Info: PME TOLERANCE                1e-06
Info: PME EWALD COEFFICIENT        0.204056
Info: PME INTERPOLATION ORDER      4
Info: PME GRID DIMENSIONS          60 54 320
Info: PME MAXIMUM GRID SPACING     1
Info: Writing FFTW data to FFTW_NAMD_2.9_Linux-x86.txt
Info: FULL ELECTROSTATIC EVALUATION FREQUENCY      4
Info: USING VERLET I (r-RESPA) MTS SCHEME.
Info: C1 SPLITTING OF LONG RANGE ELECTROSTATICS
Info: PLACING ATOMS IN PATCHES BY HYDROGEN GROUPS
Info: NONBONDED FORCES EVALUATED EVERY 2 STEPS
Info: RANDOM NUMBER SEED       686514
Info: USE HYDROGEN BONDS?      NO
Info: USING ARITHMETIC MEAN TO COMBINE L-J SIGMA PARAMETERS
Info: SUMMARY OF PARAMETERS:
Info: 8 BONDS
Info: 10 ANGLES
Info: 11 DIHEDRAL
Info: 0 IMPROPER
Info: 0 CROSSTERM
Info: 8 VDW
Info: 0 VDW_PAIRS
Info: 0 NBTHOLE_PAIRS
Info: STRUCTURE SUMMARY:
Info: 21 ATOMS
Info: 22 BONDS
Info: 27 ANGLES
Info: 33 DIHEDRALS
Info: 0 IMPROPERS
Info: 0 CROSSTERMS
Info: 0 EXCLUSIONS
Info: 63 DEGREES OF FREEDOM
Info: 21 HYDROGEN GROUPS
Info: 1 ATOMS IN LARGEST HYDROGEN GROUP
Info: 21 MIGRATION GROUPS
Info: 1 ATOMS IN LARGEST MIGRATION GROUP
```

```
Info: TOTAL MASS = 277.194 amu
Info: TOTAL CHARGE = 5.72763e-08 e
Info: MASS DENSITY = 0.000501457 g/cm^3
Info: ATOM DENSITY = 2.28776e-05 atoms/A^3
Info: ****************************
TCL: Running for 0 steps
ETITLE: TS BOND ANGLE DIHED IMPRP ELECT VDW BOUNDARY
MISC KINETIC TOTAL TEMP POTENTIAL TOTAL3 TEMPAVG
PRESSURE GPRESSURE VOLUME PRESSAVG GPRESSAVG

ENERGY: 0 9.3381 5.3578 8.6457 0.0000 38.2396
7.6439 0.0000 0.0000 17.0341 86.2593
272.1260 69.2252 86.3070 272.1260 7.0987
7.0987 917929.8396 7.0987 7.0987

Program finished.
```

NB: some of the lines were deleted for a matter of space, and the structure for the energies is distorted.
All the information about the total charge, energy, are in this file.
It also says that NAMD uses the force field CHARMMS, it just means that NAMD uses a certain way of calculating the potential energies, called CHARMMS. It calculates the energies the following way [39]:

- 2-bodies: $\Phi_{bond} = k(r - r0)^2$. k is the spring constant, r the distance between the two atoms, and r0 the equilibrium distance
- 3-bodies: $\Phi_{three-bodies} = k_\theta(\theta - \theta 0)^2 + k_{ub}(r_{ik} - r_{ub})^2$. The structure is supposed to be i-j-k $\theta 0$ and k_θ are the equilibrium angle and the angle constant, and we add a non bonding spring between i and k, with a constant of k_{ub} and an equilibrium radius of r_{ub}
- 4-bodies torsion: $\Phi_{torsion} = k(1 + cos(n\Psi + \phi)$if n ¿ 0 and $k(\Psi - \phi)^2$ if n = 0. Ψ is the angle between the plans ijk and jkl (the structure is i-j-k-l), n indicates the periodicity, k is a multiplicative constant,and ϕ is the phase shift.
- LJ: $\Phi_{Lennard-Jones}(r) = -E_{min}[(\frac{R_{min}}{r})^{12} - (\frac{R_{min}}{r})^6]$
- Coulombic:$\Phi_{elec} = \frac{Cq_iq_j}{\epsilon 0 r_{ij}^2}$. C is the Coulomb constant, q the charge and r the distance

Appendix D

Linux

A computer requires an *Operating System* (OS) in order to function. It allows the user to communicate and command the computer. This is the OS that will allow the user, or not, to do something. The main three OS are Mac OS, Windows and Linux. In opposite of the two others, Linux was designed with the idea of sharing, and of free and open source of the software. Open source means that the software source (its 'DNA') is readable by anyone, providing they have the proper knowledge and tools to do so [21]. They are also allowed to modify it. Usually it also owns a copyleft: you can download it, modify it. if at least your say where it comes from, and if anything you do on its code is also copyleft (you cannot download it, then modify the code source and then sell it, or claim it as your property) [21]. Since the history and main characteristic, which are interesting but not useful for the present work, can be easily found on the Internet, they will not be presented them. The only thing that will be presented is its logo, which is relevant and really show the spirit of Linux [21].

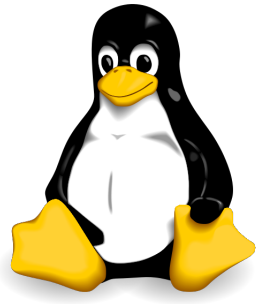

Figure D.1: Tux the penguin

It is a penguin. In 1996, a logo contest was established to give a logo to Linux, and the creator of this OS, Linus Torvalds, that like the penguins, asked that one become the logo [22]. His justification was that Linux aims are strongly related to penguins behavior. Linux aim is to satisfy the user [22]. The penguins are, according to Torvalds, satisfied globally, and very friendly, which can be checked in every zoo protecting penguins. One can basically do anything with Linux (meaning doable with a computer), one just need time, and the proper tools [22]. The friendly side comes from the fact that Linux (even if it was not true at the start), is very user-friendly, i.e. ergonomic, and easy to use. The second reason of this is that there is a big community of users, that helps each others with any of their problems. They regroup on forums, chats. And, during a snow tempest, the penguins will form a circle, the oldest, therefore theses that cannot reproduce anymore are on the outside of the circle, and

the young ones are inside, protected. People using Linux since a long time usually help the new users.
Linux is widely used as OS for super calculator and servers, due to its security [21]. Basically, this is because they are not a lot of viruses for Linux, and then because a virus would have the same right as the user (who cannot 'do' anything bad on the computer by default, for having 'full' power, one need to write the command 'sudo' for substitute user DO then a command then the personal password will be asked), so since the virus does not possess one's password, it cannot have access to sensitive information or do anything like destroy the mother board, or install other software [21].
Due to this, Linux is used by many scientists. And even chemist might need to use it (one need sometimes DFT calculations for example, even if one is an organist chemist). However, not a lot of chemist know the basis or how to deal with Linux, so some 'life saving' commands will be presented, then some more useful bash script, that can do many things; will be explained.
When using Linux, one can have a desktop windows like, or use a 'command' mode, where one only type your commands, instead of clicking [21]. Both are useful, depending on what one want to do, and if one is used to it. For example, if one want to copy paste a single file, no need to use the commands, however, if one want to copy paste all the pdf files of a specific directory, to another one, and then synchronize them, one need to use the commands [21].
The first useful commands are:

- pwd: print work directory. This command displays the current directory
- cd X: change directory X. The users moves into directory X. If only cd was used, the user goes back to the root (the initial directory), and cd .. will transfer the user back to the previous directory
- ls : list segment. It will provide the list of the files in the current directory, or if ls X is given, it will provide the list of files in the X directory

Theses are the first useful commands, that will allow you to navigate within your computer using the command mode. The next commands are basic operations:

- mkdir: make directory. mkdir X creates the directory X.
- vi file. Shortest abbreviation of visual. One 'see' the file, i.e. see what is inside (characters, digits). By default one just see, then ine can modify by pressing 'i', to 'insert', or 'r' to replace (one put the cursor on a character, press r then another character, to replace the first one by the second one). Then escape to leave the insert mode, :q to quit without saving, or :x to quit and save. By default, if the file did not exist, this command will create it and one will start editing it
- emacs file or nedit file. Theses commands are similar to 'vi', except they are more intuitive than vi, and look more like the text editor of windows, for example. One can use common commands like 'ctrl-c' 'ctrl v' to copy paste in theses editors
- tail file. Will show the tail (the last 10 lines) of the file
- head file. Similar to fail, but will display instead the first 10 lines
- less file. It will display a part of file, and using the arrows one can keep going through the document

- mv file filebis. Will move the file from any directory (just specify it: X/Y/file, to the current repertory (or any chosen repertory if indicated
- cp file file. Similar to mv, except it copies the file, instead of moving it
- rsync -vauzf X. Synchronize the current directory with the directory X, -vauzf are just options, meaning keeping the format, the date of creation, upgrade...

Theses are the basic commands, that one can use to do 'small tasks'. Using the 'bash' language, one can do more complex tasks:

- cat X $\rangle$ Y will copy X and print it in Y (if cat X $\rangle\rangle$ Y, it will be at the end of Y)
- grep ' X' file $\rangle$ filebis will look for X inside 'file' and paste it into 'filebis'
- awk will allow the user to make calculations: `awk '\{print \$6, \$7, \$8\}' inp$\rangle$ out` will take columns 6 7 and 8 in 'inp' and paste them in 'out', and `awk '\{print \$61`, $7, $8}' test $\rangle$ coordinates, will do the same, but adding 1 to the column 6
- the command `|`, called 'pipe' allows the user to make suit of commands: `inp='<for i in \$(seq10);`
  `do j=\$(printf "\%02d" \$i ); average4.awk file_\${j}.data; done | grep sigma'`
  is what was used to plot the curve $\sigma = f(thickness)$. Basically it created variables, then asked to the computer to go in the data pick sigma and created an input called 'inp' with theses sigma. The file 'inp' was then plot with GNUplot

Appendix E

LaTeX

When writing a document, one has the choice between several software, but they are divided between two major kinds: 'WYSIWYG' for 'What you see is what you get' like Word, where one sees exactly what one will print on the paper, and the software like LaTeX, that are designed to separate the form from the content [20]. In other words, in LaTeX, one only 'write', when one want [20]. To start a chapter, one write `\chapter{X}`, and then, at the end of one's work (or when one wants to test), one compile and the software will know it is a chapter, and will make the layout in function of that [20].
In fact, one's text is a kind of program, read by another program, that will do the layout, everything. One just has to worry about the text, and provide all the options one wants the layout, the type of document. Theses options are given in the beginning of the document, with the package one wants to use [20]. The package are little script one can tell LaTeX to use, to add possibilities to one's work. For example, by default, LaTeX cannot implement figures in the document, but with the package *graphicx* it can. So the beginning of one's document should look like [20]:

```
\documentclass[12pt]{report}
\usepackage[top=1.5cm, bottom=2cm, left=2.5cm, right=2.5cm]{geometry}
\usepackage{graphicx}
```

Here the document is a report, the font size is 12 pt, the top margin is 1.5 cm..... and it can implement pictures. There are packages for almost everything, for example the molecules drawn (in section 1.2.1) were drawn with the package `chemfig`, the code within a box with the package `lslisting`, and the beautiful flowchart with `tikz` [20].
Once all the options are given, one can start the document with `\begin{document}`, and write one's text (for starting a section use`\section{x}`.. one can divide the document up to subsubsections). One can add appendix with the command `\appendix`, equations with `\begin{equation}\end{equation}`, mathematics with `$...$`. One end one's document with `\end{document}` [20].
So one's document looks like:

```
\documentclass[police size]{document type}
\usepackage{A}
\usepackage{B}
\usepackage{C}
.
.
\usepackage{Z}
```

```
\begin{document}
\chapter{1}
\section{1.1}
\subsection{1.1.1}
\subsubsection{1.1.1.1}
.
.
.
\chapter{2}
.
.
.
.
\appendix
\chapter{A}
.
.
\chapter{B}
.
.
.
\end{document}
```

One can add a table of content with `\tableofcontents`, a list of figures or table with `\listoftables` or `\listoffigures`.
LaTeX is a very powerful tool, all the sections, chapters and so on are automatically labelled. One really just has to focus on one's text and ideas [20].

Bibliography

[1] B. J. Alder and T. E. Wainwright. Phase transition for a hard sphere system. *J. Chem. Phys.*, 27:1208, 1957.

[2] M.P. Allen and D.J. Tildesley. *Computer simulation of liquids*. Oxford University Press, 1989.

[3] N. L. Allinger, Y. H. Yuh, and J. Lii. Molecular mechanics. the mm3 force field for hydrocarbons. *J. Am. Chem Soc.*, 111:8551, 1989.

[4] D. Andrienko. Introduction to liquid crystals. September 14, 2006.

[5] Bideaux Anthony and Bladh Nichols. *Handbook of Mineralogy: Elements, Sulfides, Sulfosalts.* Mineralogical Society of America, 2003.

[6] D. W. Berreman. Solid surface shape and the alignment of an adjacent nematic liquid crystal. *Phys. Rev. Lett.*, 28(26):1683–1686, Jun 1972.

[7] L. M. Blinov and V. G. Chigrinov. *Electrooptic effects in liquid crystal materials*. Springer-Verlag, 1994.

[8] A. Brillante, I. Bilotti, R. G. Della Valle, E. Venuti, A. Girlando, M. Masino, F. Liscio, S. Milita, C. Albonetti, P. D'angelo, A. Shehu, and F. Biscarini. Structure and dynamics of pentacene on sio_2: From monolayer to bulk structure. *Phys. Rev. B*, 85:195308, May 2012.

[9] R. A. Buckingham. he classical equation of state of gaseous helium, neon and argon. *Proceedings of the Royal Society of London. Series A, Mathematical and Physical Sciences*, 168:264–283, 1938.

[10] S. J. Clark, M. D. Segall, C. J. Pickard, P. J. Hasnip, M. J. Probert, K. Refson, and M. C. Payne. First principles methods using castep. *Z. Kristallogr.*, 220(5–6):567–570, 2005.

[11] Polygen Corp. Parameter and topology files for charmm, 1992. Version 22, copyright.

[12] T. Darden, D. York, and L. Pedersen. Particle mesh ewald: an n.log(n) method for ewald sums in large systems. *J. Chem. Phys.*, 98:10089–10092, 1993.

[13] T. Duncan, J. M. Chen, F. K. Friedman, M. Hyde, L. Chie, and M. R. Pincus. Comparison of molecular dynamics averaged structures for complexes of normal and oncogenic ras-p21 with sos nucleotide exchange protein, containing computed conformations for three crystallographically undefined domains, suggests a potential role of these domains in ras signaling. *The Protein Journal*, Issue 3:217–228, 2004.

[14] P. Ewald. Die berechnung optischer und elektrostatischer gitterpotentiale. *Ann. Phys*, 64:253–287, 1921.

[15] J.D. Gale and A.L. Rohl. The general utility lattice program (gulp). *Mol. Simul.*, 29(5):291–341, 2003.

[16] R. G.Mortimer. *Physical chemistry*. The Benjamin/Cummings Publishing Company.Inc, 1993.

[17] M. Hird. *Physical properties of liquid crystals Vol 1: Nematics*. IEE, 2001.

[18] R.W. Hockney and J.W. Eastwood. *Computer Simulation Using Particles*. Adam Hilger, 1989.

[19] http://chemwiki.ucdavis.edu.

[20] http://en.wikipedia.org/wiki/LaTeX.

[21] http://en.wikipedia.org/wiki/Linux.

[22] http://www.generation-linux.fr/index.php?post/2009/01/28/L-histoire-de-Tux-la-mascotte-de Linux.

[23] W. L. Jorgensen and N. A. McDonald. Development of an all-atom force field for heterocycles. properties of liquid pyridine and diazenes. *Teochem. J. Mol. Struct.*, page 424:145, 1998.

[24] J.P.Michel, E.Lacaze, M.Alba, M.Goldmann, and F.Rieutord. Physisorption of 4-n-octyl-40-cyanobiphenyl (8cb) molecules on mos2: interpretation of pairing phenomenum. *Surface science*, 2002.

[25] N. Katsonis, E. Lacaze, and B. L. Feringa. Molecular chirality at fluid/solid interfaces: expression of asymmetry in self-organised monolayers. *J. Mat. Chem.*, 2008.

[26] E. Lacaze, A. Apicella, M. P. De Santo, D. Coursault, M. Alba, M. Goldmanna, and R. Barberi. Ordered interfaces for dual easy axes in liquid crystals. *Soft Matter*, 2010.

[27] Emmanuelle Lacaze, Jean Philippe Michel, Michel Goldmann, Marc Gailhanou, Marc de Boissieu, and Michel Alba. Bistable nematic and smectic anchoring in the liquid crystal octylcyanobiphenyl (8cb)adsorbed on a mos2 single crystal. *Phys. Rev.*, 69, 2004.

[28] O. Lehmann. Uber fliessende krystalle. *Zeitschrift fur Physikalische Chemie 4*, page 462?472., 1889.

[29] J. E Lennard-Jones. On the determination of molecular fields. *Proc. R. Soc. Lond.*, 106:463–477, 1924.

[30] G.R. Luckhurst, T. Miyamoto, A. Sugimura, T. Takashiro, and B.A. Timimi. The surface-induced static director distribution in thin nematic liquid crystal films: A deuterium nuclear magnetic resonance spectroscopy study. *J. Chem. Phys.*, 114(23):10493–10503, JUN 15 2001.

[31] E. R. McNellis, J. Meyer, and K. Reuter. Azobenzene at coinage metal surfaces: Role of dispersive van der waals interactions. *Phys. Rev. B*, 80:205414, 2009.

[32] D. Merki, S. Fierro, H. Vrubel, and X. Hu. Amorphous molybdenum sulfide films as catalysts for electrochemical hydrogen production in water. *Chemical Science*, 2:1262, 2011.

[33] L. Muccioli, G. D'Avino, R. Berardi, S. Orlandi, A. Pizzirusso, M. Ricci, O. M. Roscioni, and C. Zannoni. Supramolecular organization of functional organic materials in the bulk and at organic/organic interfaces. a modelling and computer simulation approach. *Top. Curr. Chem.*, to be published, 2013.

[34] S. K. Nath and R. Khare. New force field parameters for branched hydrocarbons. *J. Chem. Phys.*, 115:10837, 2001.

[35] S. Orlandi and C. Zannoni. Phase organization of mesogen-decorated spherical nanoparticles. *Mol. Cryst. Liq. Cryst.*, 573:1–9, 2013.

[36] M. F. Palermo. Atomistic simulations of bulk and free standing film smectcs. Master's thesis, Alma Mater Studiorum Universita di Bologna, 2011.

[37] P. Pasini and C. Zannoni. *Advances in the Computer Simulations of Liquid Crystals*. NATO ASI Series. Springer, 1999.

[38] J. P. Perdew, K. Burke, and M. Ernzerhof. Generalized gradient approximation made simple. *Phys. Rev. Lett.*, 77(18):3865–3868, Oct 1996.

[39] J.C. Phillips, R. Braun, W. Wang, J. Gumbart, E. Tajkhorshid, E. Villa, C. Chipot, R.D. Skeel, L. Kale, and K. Schulten. Scalable molecular dynamics with namd. *J. Computat. Chem.*, 26:1781–1802, 2005.

[40] A. Pietropaolo, L. Muccioli, R. Berardi, and C. Zannoni. A chirality index for identifying protein secondary structures. *Proteins: Structure, Function, and Bioinformatics*, 70:667–677, 2008.

[41] A. Pietropaolo, L. Muccioli, C. Zannoni, and E. Rizzarelli. Conformational preferences of the full chicken prion protein in solution and its differences with respect to mammals. *ChemPhysChem*, 10:1500–1510, 2009.

[42] A. Pizzirusso. *Computer simulation of ordering and dynamics in liquid crystals in the bulk and close to the surface*. PhD thesis, Alma Mater Studiorum Universita di Bologna, 2008.

[43] A. Pizzirusso, R. Berardi, L. Muccioli, M. Ricci, and C. Zannoni. Predicting surface anchoring: molecular organization across a thin film of 5cb liquid crystal on silicon. *Chemical Science*, 3:573, 2012.

[44] A. Pizzirusso, M. B. Di Cicco, G. Tiberio, L. Muccioli, R. Berardi, and C. Zannoni. Alignment of small organic solutes in a nematic solvent: The effect of electrostatic interactions. *J. Phys. Chem. B*, 116(12):3760–3771, 2012.

[45] E. L. Pollock and J. N. Glosli. Comments on pppm, fmm, and the ewald method for large periodic coulombic systems. *Comp Phys Comm*, 95:93, 1996.

[46] B. Radisavljevic, A. Radenovic, J. Brivio, V. Giacometti, and A. Kis. Single-layer mos2 transistors. *Nature Nanotechnology*, 6, 2011.

[47] A. Rahman and F. H. Stillinger. Improved simulation of liquid water by molecular dynamic. *J. Chem. Phys.*, 60:1545, 1974.

[48] A. K. Rappe, C. J. Casewit, K. S. Colwell, W. A. Goddard, and W. M. Skiff. Uff, a full periodic table force field for molecular mechnaics and molecular dynamics simulations. *J. Am. Chem. Soc.*, 114:10024–10035, 1992.

[49] O. M. Roscioni, L-Muccioli, R. G. Della Valle, A. Pizzirusso, M. Ricci, and C. Zannoni. Predicting the anchoring of liquid crystals at a solid surface: 5-cyanobiphenyl on ccristobalite and gglass silica surfaces of increasing roughness. *Langmuir*, 2013.

[50] H. Sunj. Compass: an ab-initio force field optimized for condensed-phase aplications overview with details on aklane and benzene compounds. *J. Phys. Chem.*, 102:7338–7364, 1998.

[51] G. Tiberio, L. Muccioli, R. Berardi, and C. Zannoni. Towards in silico liquid crystals. realistic transition temperatures and physical properties for n-cyano-biphenyls via molecular dynamics simulations. *ChemPhysChem*, 10:125–136, 2009.

[52] A C. T. van Duin, S. Dasgupta, F. Lorant, and W. A. Goddard. Reaff: a reactive for field for hydrocarbons. *J. Phys. Chem.*, 105:9396, 2001.

[53] W. F. van Gunsteren and H. J. C. Berendsen. Groningen molecular simulation (gromos) library manual. *Biomos*, Groningen, 1987.

[54] D. Vanderbilt. Soft self-consistent pseudopotentials in a generalized eigenvalue formalism. *Phys. Rev. B*, 41(11):7892–7895, Apr 1990.

[55] V. Varshney, S. S.Patnaik, C. Muratore, A. K.Roy, A. A.Voevodin, and B. L.Farmer. Md simulations of molybdenum disulphide (mos2): Force-field parametrization and thermal transport behavior. *Computational Materials Science*, 48:101–108, 2010.

[56] L. Verlet. *Phys. Rev.*, 98:159, 1967.

[57] K. Voitchovsky, J.J. Kuna, S.A. Contera, E. Tosatti, and F. Stellacci. Direct mapping of the solid-liquid adhesion energy with subnanometre resolution. *Nature Nanotech.*, 5:401–405, 2010.

[58] J. Wang, P. Cieplak, and P. A. Kollman. How well does a restrained electrostatic potential (resp)model perform in calculating conformational energies of organic and biological molecules? *J. Comp. Chem.*, 21:1049, 2000.

[59] wikipedia.org.

[60] www.mindat.org.

[61] www.webmineral.com.

[62] X. Zhuang, L. Marrucci, D. Johannsmann, and Y.R. Shen. Dependence of liquid crystal bulk alignment on its surface monolayer. *Mol. Cryst. Liq. Cryst. A*, 262:1323–1331, 1995.